Geochemistry, Geophysics, Geosystems®

RESEARCH ARTICLE
10.1029/2021GC009809

Special Section:
A fresh look at the Caribbean plate geosystems

Elongated Giant Seabed Polygons and Underlying Polygonal Faults as Indicators of the Creep Deformation of Pliocene to Recent Sediments in the Grenada Basin, Caribbean Sea

A. Gay[1], C. Padron[2,3], S. Meyer[1,4], D. Beaufort[5], E. Oliot[1], S. Lallemand[1], B. Marcaillou[4], M. Philippon[1], J-J. Cornée[1], F. Audemard[6], J-F. Lebrun[1], F. Klingelhoefer[3], B. Mercier de Lepinay[4], P. Münch[1], C. Garrocq[1], M. Boucard[1,4], L. Schenini[4], and the GARANTI cruise team

[1]Géosciences Montpellier, CNRS, Université de Montpellier, Université des Antilles, Montpellier, France, [2]Departamento de Ciencias de la Tierra, Universidad Simón Bolívar (USB), Caracas, Venezuela, [3]Géosciences Marines, Ifremer, Plouzané, France, [4]Géoazur, Université Côte d'Azur, CNRS, IRD, Observatoire de la Côte d'Azur, Valbonne, France, [5]Université de Poitiers, Poitiers, France, [6]Universidad Nacional de San Luis, San Luis, Argentina

Abstract Based on 2D seismic profiles, multibeam and seabed grab cores acquired during the Garanti cruise in 2017, 1–5 km wide seabed giant polygons were identified in the Grenada basin, covering a total area of ~55,000 km^2, which is the largest area of outcropping polygonal faults (PF) ever found on Earth so far. They represent the top part of an active 700–1,200 m thick underlying polygonal fault system (PFS) formed due to the volumetric contraction of clay- and smectite-rich sediments, initiated in the sub-surface at the transition between the Early to Middle Pliocene. The short axes of the best-fit ellipses obtained from a graphical center-to-center method were interpreted as the local orientation of a preferential contraction perpendicular to the creep deformation of slope sediments. In the North Grenada Basin, the polygons are relatively regular, but their short axes seem to be parallel to a N40°E extension recently evidenced in the forearc, possibly extending in the backarc, but not shown in the study area. They are most probably related to a progressive burial due to a homogeneous subsidence. In the South Grenada Basin, the polygons are more elongated and their axes are progressively rotating southeastward toward the depocenter, indicating a creep deformation toward the center of the basin created by a differential subsidence. Seabed polygons and underlying PF could thus be indicative of the deformation regime of shallow sediments related to main slopes controlled by two different basin architectures.

Key Points:

- Seabed giant polygons in the Grenada Basin cover the largest area (55,000 km^2) ever found on Earth
- The short axis of best-fit ellipses of polygons may represent the orientation of the creep deformation of slope sediments
- The north and south tectonic domains in the Grenada Basin are marked by major differences in the shape and orientation of seabed polygons

Correspondence to:
A. Gay,
aurelien.gay@umontpellier.fr

Citation:
Gay, A., Padron, C., Meyer, S., Beaufort, D., Oliot, E., Lallemand, S., et al. (2021). Elongated giant seabed polygons and underlying polygonal faults as indicators of the creep deformation of Pliocene to recent sediments in the Grenada Basin, Caribbean Sea. *Geochemistry, Geophysics, Geosystems*, *22*, e2021GC009809. https://doi.org/10.1029/2021GC009809

Received 29 MAR 2021
Accepted 29 OCT 2021

Author Contributions:
Conceptualization: A. Gay, C. Padron, S. Meyer
Formal analysis: A. Gay, D. Beaufort, S. Lallemand, J-J. Cornée
Funding acquisition: S. Lallemand, J-F. Lebrun, P. Münch
Investigation: A. Gay, C. Padron
Methodology: A. Gay, S. Meyer, D. Beaufort, E. Oliot
Project Administration: S. Lallemand, J-F. Lebrun, P. Münch

1. Introduction

Polygonal fault systems (PFS) have been recognized in many basins worldwide (Cartwright, 1994, 2011; Cartwright & Dewhurst, 1998; Clausen et al., 1999; Clausen & Korstgård, 1993; Gay & Berndt, 2007; Gay et al., 2007, 2004; Ghalayini & Eid, 2020; Hansen et al., 2004; He et al., 2010; Klitgord & Grow, 1980; Laurent et al., 2012; Lonergan et al., 1998; Oldham & Gibbins, 1995; Sun et al., 2010). They are a special type of non-tectonic normal faults forming polygons in plan view and prisms in 3D. Four main hypotheses have been proposed to explain PFS formation: (a) syneresis related to colloidal properties of fine-grained sediments (Dewhurst et al., 1999), (b) density inversion and associated hydrofracturing (Watterson et al., 2000), (c) smectite-rich clays causing residual friction at low burial depth (Goulty, 2002, 2008) and (d) grain dissolution in uncemented media inducing a decrease in horizontal stress that leads to shear failure and shear strain localization (Cartwright, 2011; Shin et al., 2008, 2010). Additionally, Gay and Berndt (2007) have proposed that sediment loading may also play a role in the initiation, propagation and reactivation of polygonal faults (PF). Geometries of PFS suggest a heterogeneous volumetric compaction (shrinkage in plan view) accommodated by small scale normal faults (Davies et al., 2009; Gay et al., 2004; Ireland et al., 2011; Neagu et al., 2010; Wrona et al., 2017).

PFS are usually interpreted as layer-confined because they occur within buried sub-horizontal intervals, a few hundreds of m thick, associated with lithological variations of the host sediments. They sometimes abruptly end at a specific stratigraphical horizon but they can locally connect to major faults deforming the basin (Gay et al., 2007). Some of these faults almost reach the modern seabed, thus representing the top of a modern or recently active PFS (Hansen et al., 2005; Ireland et al., 2011). Although many PFS are buried to depths of a few tens of meters to hundreds of meters, only a few examples have been reported to crop out at the present-day seabed

Resources: A. Gay, M. Boucard, L. Schenini
Software: C. Padron, B. Mercier de Lepinay, C. Garrocq
Supervision: A. Gay, J-F. Lebrun
Validation: C. Padron, J-F. Lebrun
Visualization: C. Garrocq
Writing – original draft: A. Gay, C. Padron
Writing – review & editing: E. Oliot, S. Lallemand, B. Marcaillou, M. Philippon, J-J. Cornée, F. Audemard, F. Klingelhoefer

such as in the Hatton Basin (Berndt et al., 2012) and in the Norway Basin (King & Cartwright, 2020; Laurent et al., 2012).

In the investigated area, extending from the Saba Bank southwest of Virgin Islands in the north Grenada Basin (NGB) to the south Grenada Basin (SGB) west off Grenada island, the Grenada Basin is geographically located in the backarc basin of the subducting North American Plate beneath the Caribbean Plate (Figure 1). Giant polygons, 1–5 km wide, have been identified outcropping at the seabed during the GARANTI Cruise in May−June 2017. They cover the largest area of outcropping polygonal faults ever found on Earth, covering a surface area of ∼55,000 km^2. They are directly linked to a unique underlying 700–1,000 m thick PFS interval that thins toward the modern volcanic arc where it abruptly ends and toward the North where sedimentary sequences are getting thinner. However, the PFS also extends toward the Venezuela Basin, west of the Aves Ridge, covering a total area of ∼75,000 km^2 in the study area, suggesting that its total extent is probably larger.

Many studies have attempted to link PFS with structural context using topology of the faults (Morley & Binazirnejad, 2020 and references therein) and/or rose diagram orientations (Jitmahantakul et al., 2020 and references therein). Even if the fault pattern can be influenced by the slope of underlying units, causing different amounts of horizontal stress anisotropy within the faulted units (Li et al., 2020), a variation from true polygonal orientation may show that the polygonal fault network is responding to local stress field perturbation (Carruthers et al., 2013; Ghalayini et al., 2017; Ho et al., 2018). Submarine slopes are submitted to elastic deformation of sediments under constant load and very low deformation rates leading to creep mechanisms, usually in clays (Hill et al., 1982). Creep would be expected to produce fault strikes (or fractures) preferentially aligned perpendicular to the direction of slow sliding with faults dipping toward the depocenter or in the direction of the regional slope (Mulder & Cochonat, 1996; Shillington et al., 2012). Such discrete faults generally lead to the formation of seafloor ridges and troughs (Cattaneo et al., 2004) or furrows (Gay et al., 2004).

The large extent of acquired data in the Grenada Basin provides a unique opportunity to investigate whether the PFS development is related to creep deformation of the sedimentary cover by using the graphical center-to-center method applied to adjacent polygons (Fry, 1979). This method allowed to better describe both the average shape of polygons and their general spatial organization. This study has shown that the Pliocene to recent sediments of the Grenada Basin are affected by two kinds of PF in the north and the south, corresponding to two previously identified tectonic domains with very different basin morphologies. PFS could be used as markers at a basin scale of the deformation regimes of shallow sediments related to main slopes controlled by different basin architectures.

2. Data and Methods

Deep-penetration multichannel seismic reflection (MCS) data were acquired onboard *R/V L'Atalante* during the GARANTI cruise in 2017 (Lebrun & Lallemand, 2017) (Figure 1). MCS data were collected using a 6,473 in^3 airgun array of 16 seismic sources emitting signals with a 9–40 Hz frequency range, and a 4.5 km long, 720-channel solid streamer. The data were quality-controlled and binned in common midpoint (CMP) gathers every 12.5 meters using the SolidQC software of IFREMER and they were processed using the Geovation Software. The seismic amplitudes were gained and centered to ±12,000. EM122 multibeam bathymetric data and high-resolution CHIRP profiles (amplitudes are 0 to 6.10^5) were also recorded along all seismic profiles. Additional profiles BOL30, 124VB-11 and 124VB-12 (Aitken et al., 2011) were used to connect our interpretation with previous studies in the SGB (Figure 1).

Clay mineralogy of grab core samples GR-07 and GR-08 collected at seabed during the GARANTI cruise (Figure 1) was determined from X-ray diffractograms of oriented powder mounts of the bulk material and the less than 2 µm granulometric fraction which is usually considered as representative of the clay fraction of sedimentary rocks. Oriented preparations are a prerequisite for a detailed characterization of the d00 reflections of phyllosilicates. The disaggregation of the bulk sediments and the dispersion of clay particles was made by ultrasonic treatment in distilled water without any preliminary grinding to strongly limit the contamination with fine grained fragments of detrital minerals. The less than 2 µm fraction was then extracted from the previous suspension by centrifugation. X-ray diffractograms were acquired on a Bruker D8 Advance diffractometer (40 kV and 40 mA) coupled with a copper anticathode (Cu Kα^{1+2} radiation) in the 2-30°2Θ angular range with 0.02°2Θ steps and a counting time of 2 s per step. Relative humidity was not controlled during data acquisition.

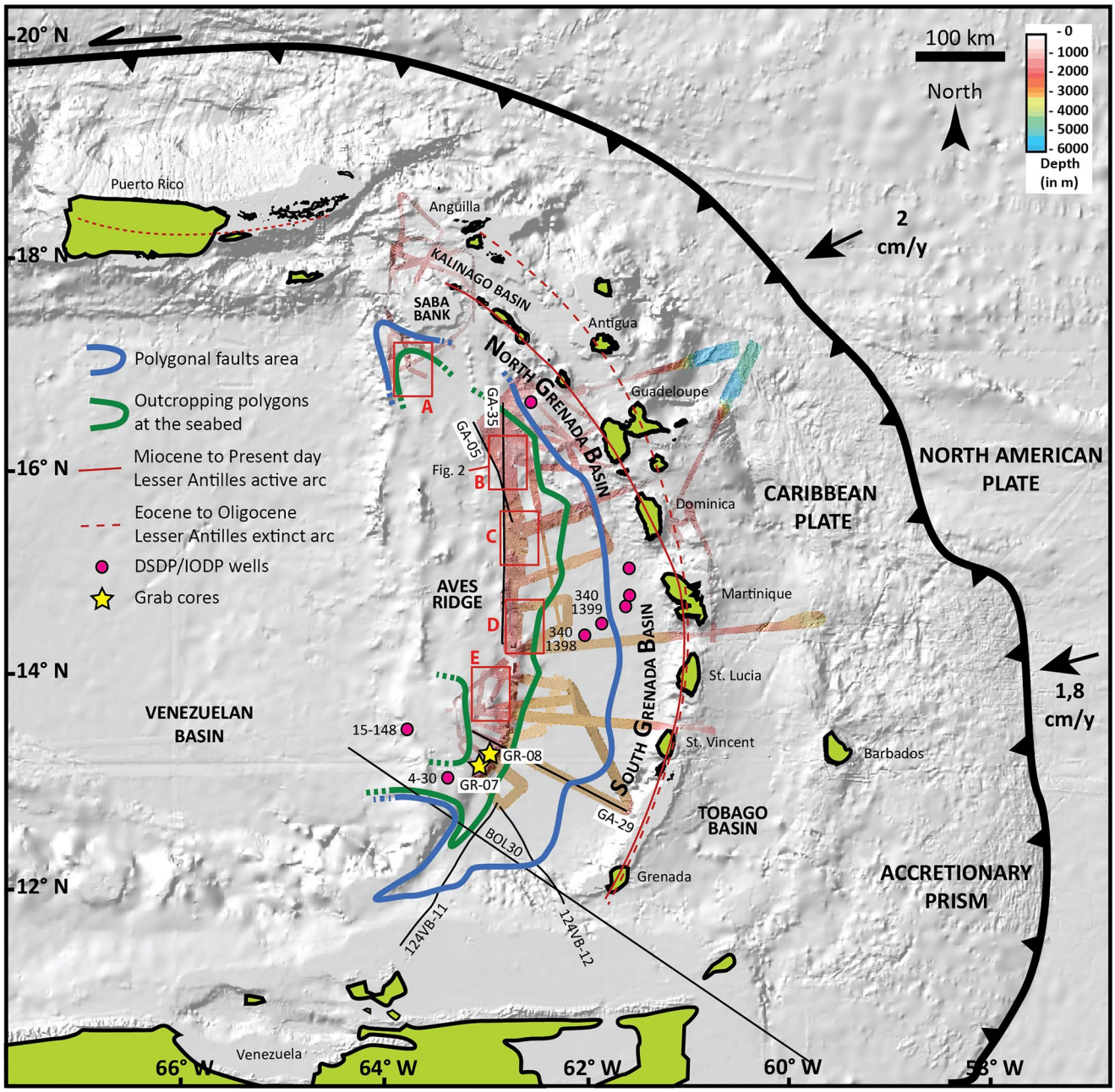

Figure 1. Regional map of the eastern Caribbean Sea displaying the extension of giant seabed polygons (green line) and underlying polygonal faults (blue line) developing in the north Grenada Basin (NGB) and the south Grenada Basin (SGB). The multibeam bathymetry data and corresponding MCS profiles (noted GA-) were acquired during the GARANTI cruise in 2017. Additional seismic profiles BOL30, 124VB-11 and 124VB-12 (Aitken et al., 2011) were used to extend the interpretation in the south. The grab cores GR-07 and GR-08 were collected within the area of seabed polygons. The shaded relief map is extracted from GEBCO datasets.

SEM observation of clay particles in sediments was performed on freshly broken fragments of core previously coated with a carbon film using a JEOL JSM IT500 scanning electron microscope equipped with secondary electron (SE), backscatter electron (BSE) detectors and coupled with a Bruker linxeye energy dispersive X-ray spectrometer (EDX). The analytical conditions for quantitative EDX analysis of clay minerals were as follow: acceleration voltage 15 kV, current beam 1 nA, counting time 60 s, working distance 11 mm, and analytical area of ~2 µm. The standards used for the EDX quantitative analysis consisted of albite (Na, Al, Si), almandine (Mg, Fe), diopside (Ca), orthoclase (K) and spessartite (Mn). Matrix corrections were performed using the PhiRhoz

mode (an evolution from ZAF methods) that is particularly efficient for light elements analysis (Packwood & Brown, 1981). The reproducibility of the standard analyses was 1.5% for all chemical elements, except Na, for which the reproducibility was 3%.

From north to south, five subzones (A to E) (Figure 1) have been selected based on available data (seismic profiles, multibeam bathymetry and CHIRP profiles) in order to perform a statistical analysis on the length and orientation of polygon edges. The furrows were first manually traced in QGIS using the deepest point between two adjacent polygons. The obtained lines were then automatically extracted and analyzed using the functions "$length" and "orientation." The results were then plotted in a rose diagram and orientations were grouped by colors every ±10° using an average distribution, which is a classical approach in characterizing a network of polygonal faults. However, although three main directions and corresponding lengths were identified (i.e., forming an average polygon in each subzone), this approach is not representative of the distribution of polygons. In order to better constrain both the shapes and the distribution of polygons, we used the mathematical center-to-center method, similar to the method proposed by Fry (1979): the distances between every pair of polygons were measured and plotted on a polar diagram using the GeoFryPlot software maintained by Rod Holcombe (https://www.holcombe.net.au/software/geofryplots.html). It computationally mimics the manual method described by Fry (1979) in which, successively, every point in the cluster takes the central position and every other point is plotted relative to that position. The relative positions of all surrounding objects are plotted until a central vacancy field emerges, defining an ellipse. The method requires the assumption that all measured objects are adjacent to their neighbors. This method provides 4 main end members: (a) Polygons are irregular with various shapes: No ellipse is found, (b) polygons are all regular: The best fit ellipse is a circle, (c) polygons are irregular with an elongated shape but they are equally distributed: the best fit ellipse is a circle and (d) polygons are irregular and all oriented: a best fit ellipse emerges with short and long axes. The center-to-center method allows the identification of both an anisotropy in shape of polygons and a preferential orientation, which are not dependent on the size of polygons. Normal PF orientations and lengths highlight the local stress state acting in the sedimentary cover in the basin (Cosgrove, 1997). Thus, the shape anisotropy of seabed polygons, evidenced by the calculated 2D best-fit ellipses, signifies a dominance of parallel and subvertical extensional faults opening against the least principal stress σ3. The long axes of ellipses are thus interpreted as representative of the mean strike of the main normal PF, and the short axes are characteristic of the maximum extension direction.

2.1. Geological Setting

The present-day crescent-shaped Grenada Basin (according to Mann, 1999 and Picard et al., 2006) results from the last 56-Ma evolution of the Caribbean plate movement forming the Greater Arc of the Caribbean (GAC) subduction zone (Audemard et al., 2009; Boschman et al., 2014; Iturralde-Vinent & MacPhee, 1999; Ladd & Sheridan, 1987; Legendre et al., 2018; Münch et al., 2014; Pindell et al., 2012). It is bounded to the west by the Aves Ridge, to the east by the Lesser Antilles Arc (LAA), to the south by the shallow Venezuelan continental shelf and to the north by the Saba Bank (Figure 1). Currently, the American plates are subducting below the Caribbean plate at a mean rate of 2 cm/y (DeMets et al., 2000). The LAA subduction zone marks the eastern boundary of the Caribbean Plate, whereas the Aves Ridge corresponds to the southern part of the remnant GAC that was exposed between approximately 88 and 59 Ma (Fox et al., 1971; Bouysse et al., 1985; Bouysse & Westercamp, 1990; Neill et al., 2011). The Grenada Basin has long been considered a typical backarc basin between the Aves Ridge and the LAA. Although it is now admitted that Grenada and Tobago basins were the same basin before they split out (Aitken et al., 2011), the present-day volcanic arc separated them with the Grenada Basin remaining in a backarc position whereas the Tobago Basin is now in a forearc position (Garrocq et al., 2021) (Figure 1). The morphology of the Grenada Basin varies from a rough ∼1,000–2,000 m deep bathymetry and a Moho ∼25 km deep in the North and a flat ∼3,100 m bathymetry and a ∼10–15 km deep Moho in the South (Gómez-García et al., 2019; Padron et al., 2021) (Figure 1). This is a marginal basin partly underlain by oceanic crust (Allen et al., 2019; Christeson et al., 2008; Padron et al., 2021), adjacent to an oceanic island arc, that receives volcaniclastic debris from the bordering volcanic arc and, to a lesser degree, the remnant arc (Carey & Sigurdsson, 1984; Murray et al., 2018; Parra et al., 1986). However, previous sedimentological and geochemical studies have indicated that Grenada Basin sediments originated from two principal sources: volcanogenic material from the LAA, and terrigenous material eroded from the South American continent (Bowles & Fleischer, 1985; Kinder et al., 1985; Parra et al., 1986; Pautrizel & Pons, 1981). Except for direct ash-fall deposits, the recent sediments in the flanks of the Grenada Basin are composed of volcanogenic debris emplaced by turbidity currents and debris-flows coming

from both the LAA (Brunet et al., 2016; Carey & Sigurdsson, 1978, ; Deplus et al., 2001; Le Friant et al., 2020; Seibert et al., 2020; Sigurdsson et al., 1980) and from the Aves Ridge (Bader et al., 1970; Holcombe et al., 1990). The hemipelagic sedimentation mixing dispersed ash and clastic clays coming from South America is the dominant process in the deeper part of the Grenada Basin (Sen Gupta et al., 1982), entering the Grenada basin by northward flowing Caribbean ocean currents (Corredor et al., 2004).

2.2. Seabed Giant Polygons and Related Normal Polygonal Faults

Seabed polygons are separated from the neighboring polygons by 700–1,500 m wide and 10–60 m deep furrows (compared to the regional seafloor) with a flat bottom (Figure 2a). The polygons are ranging from 2,000 to 3,000 m on average. However, in the SGB the seabed polygons are wider by a factor of 50%–100% where they can reach 5,000 m, suggesting that the size of polygons depends on the location within the basin.

On profile AB (GA-35 close-up view in sub-zone B), seafloor furrows are 40–60 m deep and 800–1,500 m wide depressions at the upper tips of sets of normal conjugated faults (Figure 2b). The distributed throws, typically a few tens of ms TWT along the faults form mini-grabens and the resulting depressions affect underlying horizons down to 200–300 ms TWT below seafloor. The interval affected by these small-scale normal faults is 700–1,200 ms TWT thick. On the high-resolution Chirp profiles, even considering the imprecision due to a 20X vertical exaggeration, the polygons have very steep sides, ∼3° compared to the smooth regional slope of 0.3° (Figure 3a). Very high amplitude reflections occur right beneath the seabed creating large hyperbolae. A seismic profile displayed at the identical horizontal scale shows that each depression is bounded by faults reaching the seabed (Figure 3b). The polygonal faults are characterized on seismic profiles by an intense dimming of reflections on both edges of the fault planes suggesting that fluids are the main cause for such amplitude anomaly.

In more details, the offset along the fault planes decreases both upwards toward the seabed, and downwards toward the base of the PFS where they die out. At depth, below the PFS, the horizons do not appear affected (Figure 4). The difference between the real point of max throw (up to a few tens of meters) usually identified in 3D seismic datasets (Berndt et al., 2012; Gay & Berndt, 2007; Laurent et al., 2012) and the random intersection of the seismic profile with the fault plane (giving an apparent max throw) is not significant in a 1,000 m thick interval. The maximum throw occurs at ∼450–500 ms TWT below seafloor along profile GA-05 (Figure 4). This depth corresponds to the transition between Early and Middle Pliocene, as found in the entire area from North to South.

The polygons in the sub-zones A and B are very similar in size and shape (Figures 5a and 5b). However, the bounding furrows are 10–15 m deep in sub-zone A and 40 m deep in sub-zone B compared to the regional seafloor. They are characterized by 3 main directions oriented N170-N10°E, N30-50°E and N90-110°E, with lengths of 1,260/1,274, 1,190/1,208 and 1,345/1,374 ± 15 m respectively. The average shape is a polygon with a long axis of ∼2,400/2,500 m in length in sub-zones A and B. The best-fit ellipse obtained from the center-to-center method shows a short axis oriented N40°E in both sub-zones A and B.

Sub-zone C is characterized by furrows oriented N170−10°E, N30−50°E and N70−90°E with lengths of 1,070, 1,274 and 1,047 ± 15 m respectively (Figure 5c). This defines an average polygon with a long axis of ∼2,250 m in length and 40–60 m deep bounding seafloor furrows. The best-fit ellipse calculated from the center-to-center method displays a short axis oriented N120°E.

Sub-zone D is characterized by furrows oriented N10–30°E, N30-50°E and N70–90°E with lengths of 1,245 m ± 15 m for every direction (Figure 5d). This defines average elongated polygons with a long axis of ∼3,100 m in length and 30 m deep bounding seafloor furrows. The best-fit ellipse obtained from the center-to-center approach has a short axis striking N144°E.

Sub-zone E displays furrows oriented N30–50°E, N50–70°E and N70–90°E with lengths of 1,653, 1,935 and 1,677 ± 15 m respectively (Figure 5e). This defines a very elongated average polygon with a long axis of ∼5,000 m in length, clearly visible on the bathymetric map. The seafloor furrows are 20–30 m deep. The best-fit ellipse obtained from the center-to-center method is characterized by a short axis oriented N163°E.

In the NGB the polygons are very similar in shape and orientation as shown by the ellipses obtained from the center-to-center method with a short axis oriented N40°E, whereas in the SGB, the polygons are more elongated and their orientation progressively rotates southwards, which is consistent with the orientation of the short axes of ellipses. Seafloor furrows are deeper in the north than in the south by a factor of two. Consequently, two main

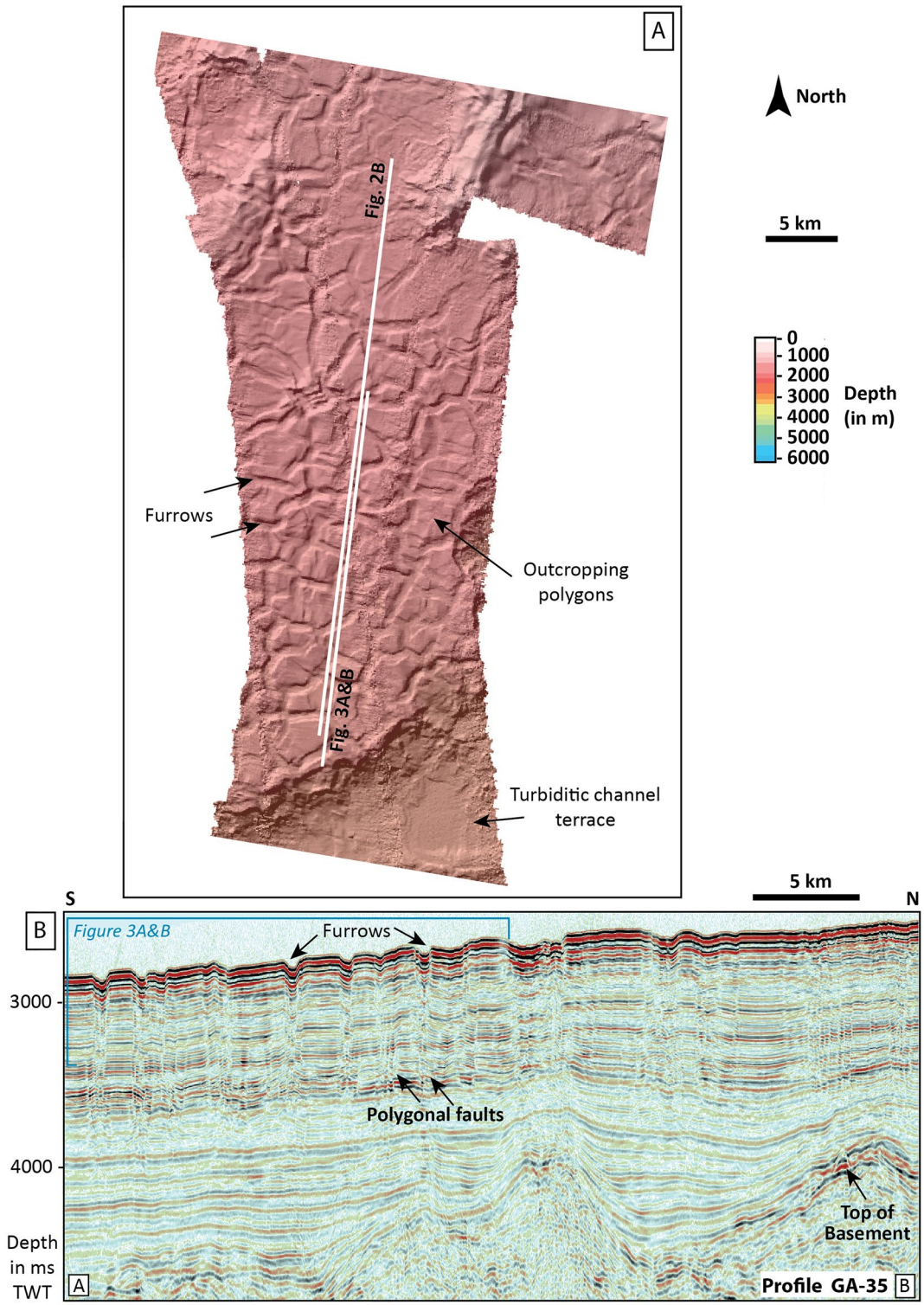

Figure 2. (a) Shaded relief map of seafloor from multibeam data along the seismic profile GA-35 showing 2–3 km wide polygons bounded by ~40 m deep furrows. (b) Seismic profile AB (GA-35 close-up view) displaying polygonal faults affecting a ~1,000 ms TWT thick interval. The polygonal faults are organized in set of small-throw normal and conjugated faults beneath seafloor furrows. The distributed small throws along the faults form mini-grabens visible down to 200–300 ms TWT below seafloor.

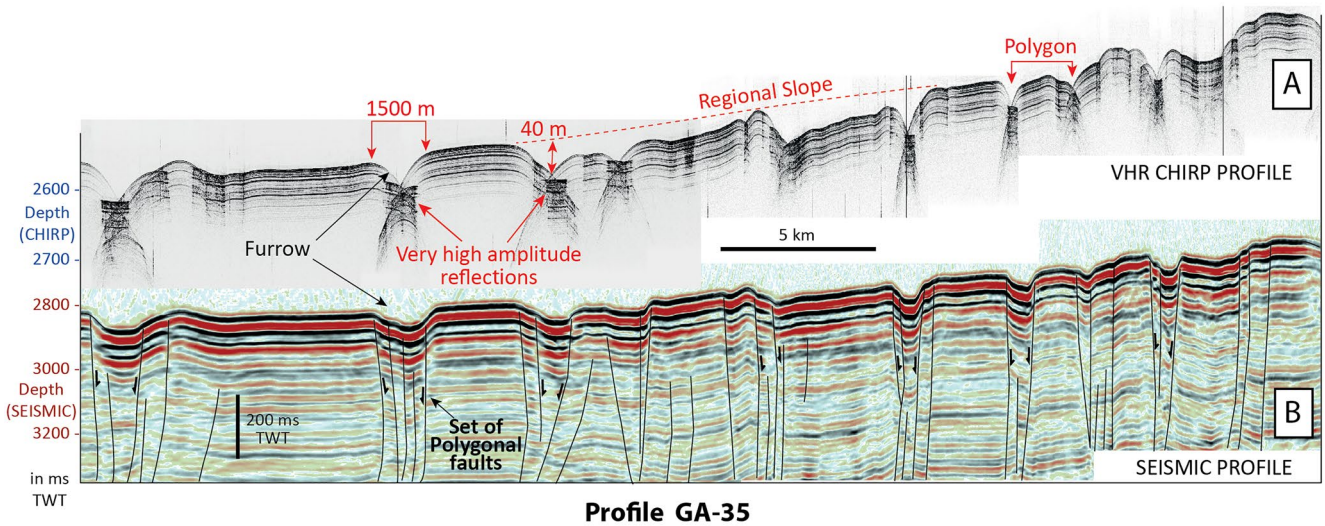

Figure 3. Very high-resolution seismic profile (CHIRP) at the identical horizontal scale than the corresponding seismic profile GA-35. The furrows are affecting the present-day seafloor and they are ~1,500 m wide and ~40 m deep (calculated with a velocity of 1,500 m/s in water). The difference in time arrival at the seabed between CHIRP and SEISMIC profiles comes from the acquisition. The seabed furrows represent the top of an underlying polygonal fault system. The bottom of furrows is characterized by very high amplitude reflections compared to well-bedded horizons between furrows.

areas are defined in the Grenada Basin in the north and the south by both the general shape of polygons and the orientation of the short axis of the best-fit ellipse calculated from the center-to-center method.

2.3. Nature, Provenance of Sediments and PF Occurence

The Pliocene-to-recent Antillean sediments are mainly of mafic-affinity, rich in pyroxenes and amphiboles but poor in quartz and biotite (in agreement with the andesitic composition of the volcanogenic material related to the LAA activity), whereas the South American supply is essentially of felsic-affinity, composed of quartz and phyllosilicate minerals, such as biotite, muscovite, and chlorite (Pautrizel & Pons, 1981). Clay mineralogy of two seabed grab cores (GR-07 and GR-08) collected during the GARANTI cruise display very similar patterns. The bulk analysis shows a high clay content, mostly composed of smectite, illite/muscovite and kaolinite with

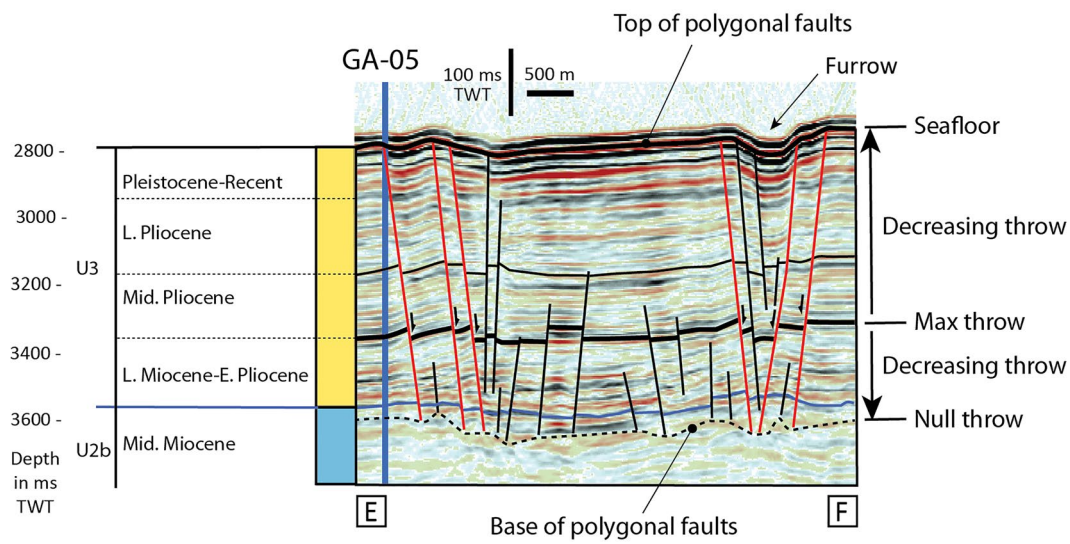

Figure 4. Detailed view of seismic profile GA-35 displaying decreasing offsets along fault planes both upward and downward. The maximum throw is located at the transition between Early and Middle Pliocene all over the Grenada Basin. Units were correlated and described in Garrocq et al. (2021).

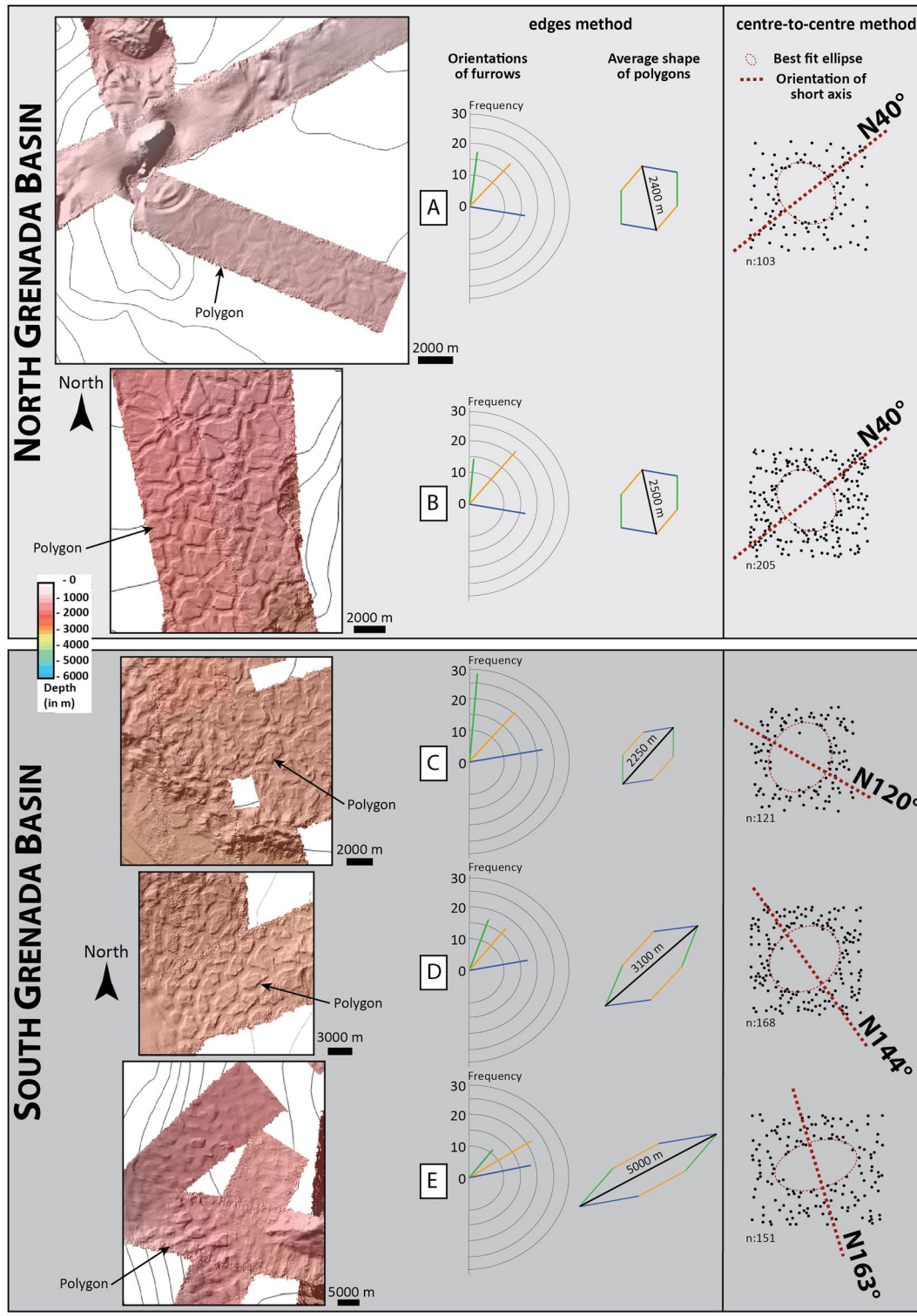

Figure 5. Left: Close-up views of seafloor polygons from multibeam data in sub-zones A to E and corresponding rose diagrams. Polygons are very similar in size and shape in sub-zones A and B in the NGB, although they are longer from sub-zone C to E toward the SGB. An average polygon is displayed based on both the main orientations of polygon edges and their lengths. Right: the best-fit ellipses, calculated from the graphical center-to-center method, provides short axes oriented N40°E in sub-zones A and B, whereas they are rotating from N120°E in sub-zone C to N144°E in sub-zone D and N163°E in sub-zone E

subordinate chlorite and pyrophyllite, mixed with non-clay minerals such as pyroxenes, plagioclases, quartz and calcite (Figure 6a). The disappearance of chlorite and pyrophyllite X-ray reflections as well as the strong decrease in the peak intensity of illite/muscovite present in the XRD pattern of the fraction <2 μm indicate that these minerals are coarse grained and probably related to a clastic metamorphic-derived source (Figures 6b and 6c). The XRD patterns of the <2 μm fraction are similar for both samples, with a very high smectite content and lower amounts of kaolinite and illite/muscovite. Based on cation exchange capacity measurement for the bulk material, the smectite content has been estimated to about 50% in both samples.

The SEM photographs shows that the sediments are dominated by smectite and kaolinite (Figures 7a and 7b). The calcite content is provided by the pelagic sedimentation of foraminifers although other minerals, such as feldspars (plagioclases), pyroxenes and quartz represent a minor contribution. The collected seabed sediments are primarily composed (>50%) of smectite at both grab core locations.

Chemical point analyses of the clay particles observed with SEM indicate that smectite is dioctahedral and is rich in Al and Fe with a layer charge mostly satisfied by K in interlayer position (Figure 7c). Such a chemical composition is similar to that of the potassic ferriferous beidellites characterized in the volcanogenic clay material in recent marine sediments (Desprairies & Bonnot-Courtois, 1980; Parra et al., 1985). In these sediments, smectite is generally derived from the diagenetic transformation of volcanogenic material (including volcanic ashes) into clay minerals. Conversely, kaolinite is usually derived from the weathering or the hydrothermal alteration of Al-bearing silicates in low pH environments and it is considered as a clastic material in marine sediments.

The hemipelagic sedimentation mixing dispersed ash and clastic clays is active since middle Miocene (Aitken et al., 2011) defining unit U3 (Figure 8). It has been identified on seismic sections as chaotic and semi-continuous tabular high amplitude reflectors (Garrocq et al., 2021). The LAA is composed of mostly andesitic igneous rocks (MacDonald et al., 2000) whose weathering products carry a distinctive signature. Smectites and kaolinite are the dominant clay minerals produced by the weathering of Lesser Antillean igneous rocks, with over twice as much smectite produced as kaolinite. Another typical weathering characteristic of an igneous island arc terrane is the absence of illite or illite-smectite mixed layers. Hydrothermal illite and illite-smectite mixed-layers may form in the geothermal fields related to the volcanic activity, as documented on the islands of Guadeloupe to Grenada (Mas et al., 2003, 2006; Murray et al., 2018; Parra et al., 1986). However, the spatial extension of geothermal areas is too limited to exert a significant contribution to clay material accumulated in marine sediments. Hence, high smectite and low illite contents are typical of sediments with a volcanogenic (Lesser Antillean) source (Parra et al., 1986; Pautrizel & Pons, 1981). Crustal terranes of the South American continent made of granites and gneisses act as the source area for non-volcanic abiogenic sediments deposited in the Caribbean. Tropical weathering of these continental rocks produces four dominant clay minerals: illite, kaolinite, smectites, and chlorite. This fine-grained terrigenous material is carried in suspension to the southeast Caribbean by major rivers, particularly the Amazon and the Orinoco (Bowles & Fleischer, 1985). Thus, a clay mineral assemblage characterized by high abundances of illite, kaolinite, chlorite and minor pyrophyllite is typical of a South American terrigenous source, as is the presence of detrital quartz (Pautrizel & Pons, 1981). Some deep channels across the Aves Ridge permitted the transport of the Venezuela Basin bottom water (commonly labeled Caribbean bottom water or CBW) into the Grenada Basin (Kinder et al., 1985).

Unit U2 (Early To Middle Miocene) was fed by the Orinoco whereas its delta front was oriented North-South toward the Grenada basin (Escalona & Mann, 2011; Xie et al., 2010). During Tertiary times the Orinoco drainage basin and its associated delta has migrated eastward over more than 500 km because of eastward deformation in north Venezuela due to the Caribbean plate/South America relative movements (Audemard et al., 2009; Beck et al., 1990; Pindell et al., 2006). Presently, the turbidite system issued from the present-day Orinoco delta develops at the eastern edge of the East Caribbean active margin partly above the large southern part of the Barbados accretionary prism and downslope at the front of this prism, within the Demerara abyssal plain (Deville et al., 2015). Unit U2 is marked by a shallowing of the facies corresponding to a progressive infilling of the Grenada Basin (Garrocq et al., 2021). Sediments in Unit U1 are deep-water, pelagic and volcanogenic shale and siltstone, with some biogenic limestone in the deeper parts (Ysaccis, 1997), whereas seismic reflections in Unit U0 are very chaotic but they are well organized in some places, possibly related to Cretaceous sediments.

In the NGB, the polygonal faults reach the seafloor, except in the vicinity of deep turbiditic channels where they do not develop at all (Figure 8a). The PFS is getting progressively thicker southward as its base is getting deeper.

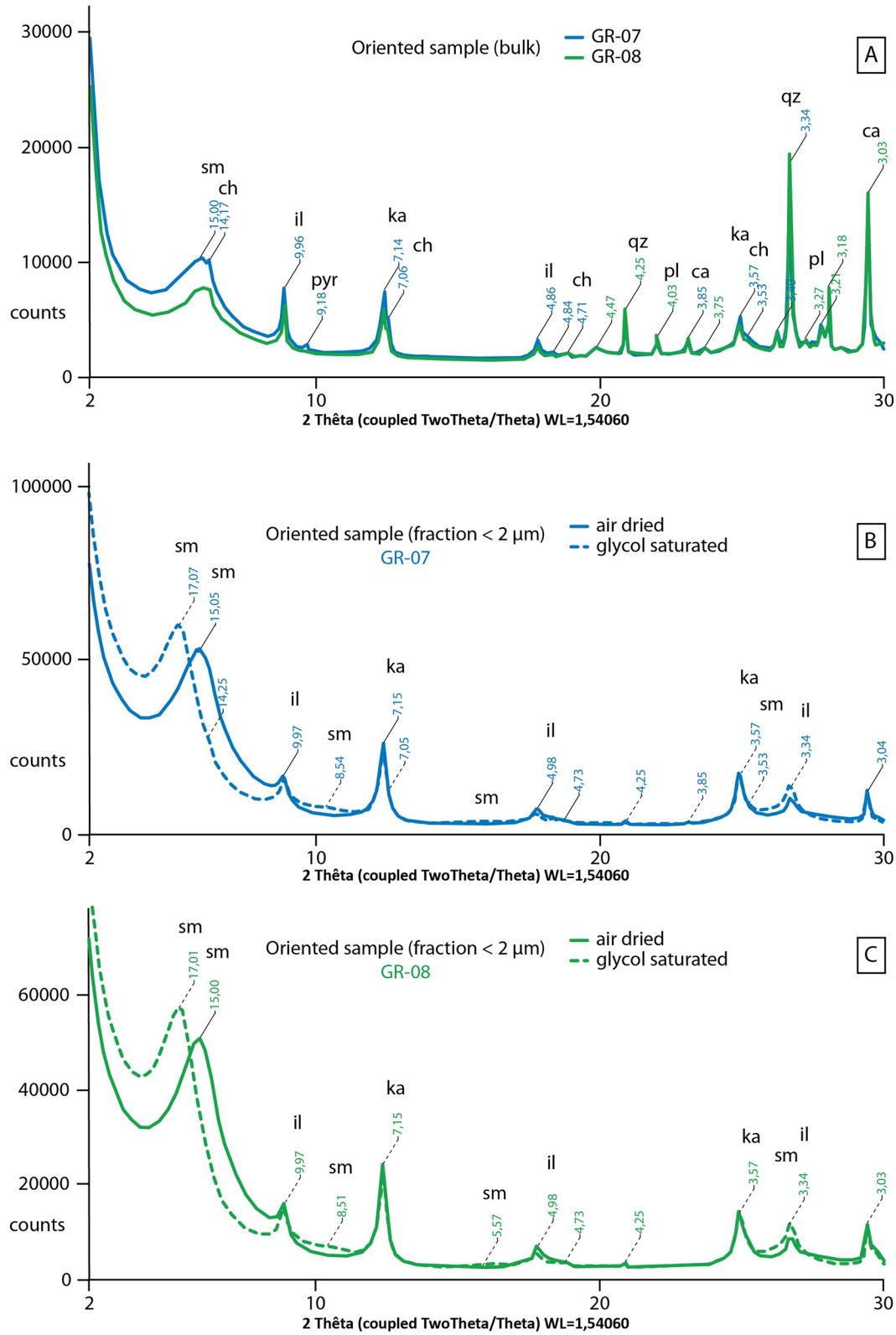

Figure 6. XRD analysis of grab cores GR-07 and GR-08. (a) bulk analysis displaying very similar patterns with a high clay content (smectite: sm, illite: Il, chlorite: ch and kaolinite: ka) and some other minerals (pyroxenes: py, plagioclases: pl, quartz: qz and calcite: ca). (b and c): analysis of the fraction <2 µm for both samples GR-07 (blue curves) and GR-08 (green curves) respectively, displaying very high smectite content, high kaolinite peaks and low illite peaks.

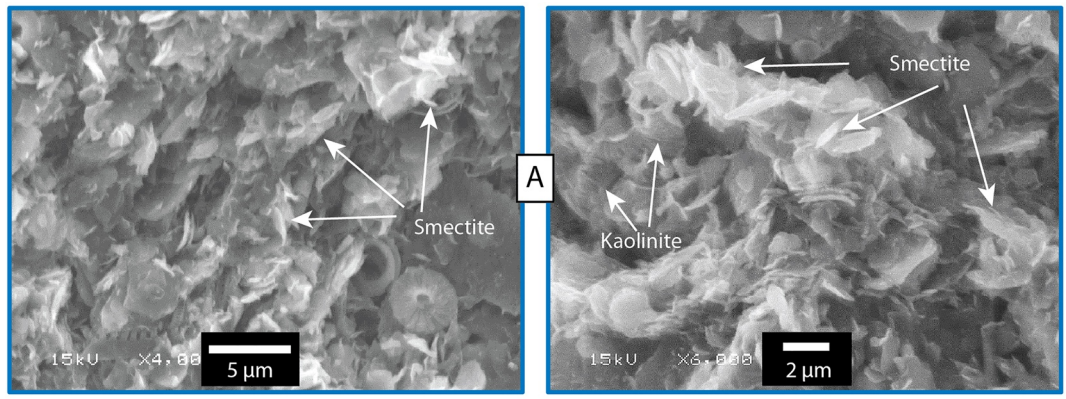

	GR-07	GR-08
SiO_2	48.57	46.36
Al_2O_3	19.65	19.84
Fe_2O_3	7.12	10.17
MgO	2.53	2.13
TiO_2	0.12	0.21
MnO	0	0
CaO	1.2	1.49
Na_2O	0.08	0.08
K_2O	3.13	3.16
Total	82.4	83.44
Number of cations (basis 11 oxygens)		
Si	3.63	3.48
Al^{IV}	0.37	0.52
Al^{VI}	1.36	1.24
Mg	0.28	0.24
Fe^{3+}	0.4	0.57
Ti	<0.01	0.01
Mn	0	0
∑oct	2.04	2.06
Na	0.01	0.01
Ca	0.1	0.12
K	0.3	0.3

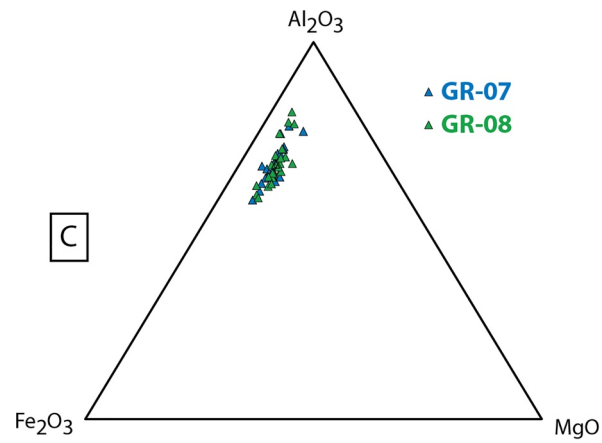

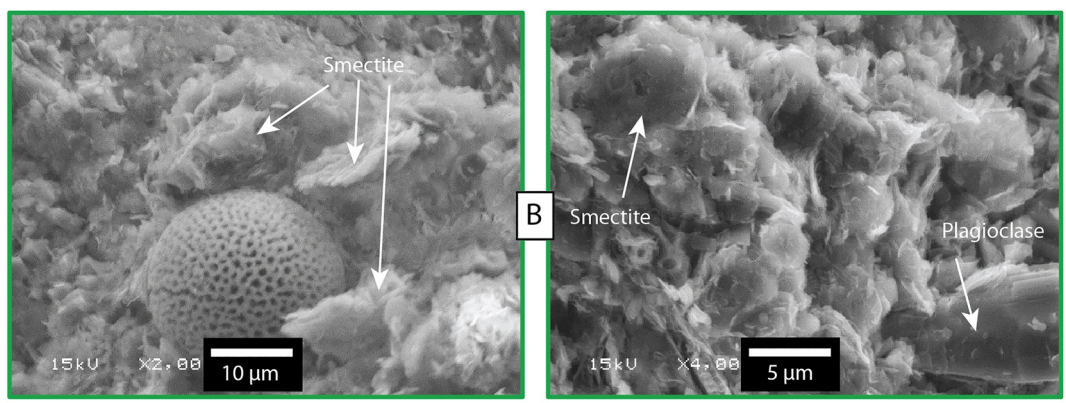

Figure 7. (a and b) SEM photographs of samples GR-07 (blue) and GR-08 (green) respectively. Both samples are dominated by smectite and kaolinite but smectite represents more than 50% of the bulk volume. The calcite peaks are derived from pelagic foraminifers; (c) (left): Representative chemical analyses of smectites and the corresponding calculated structural formula. Total iron was arbitrarily considered as Fe^{3+}; (right): Al_2O_3-Fe_2O_3-MgO plots of the point chemical analyses of smectite particles from the two grab cores (GR-07 and GR-08) collected during the GARANTI cruise.

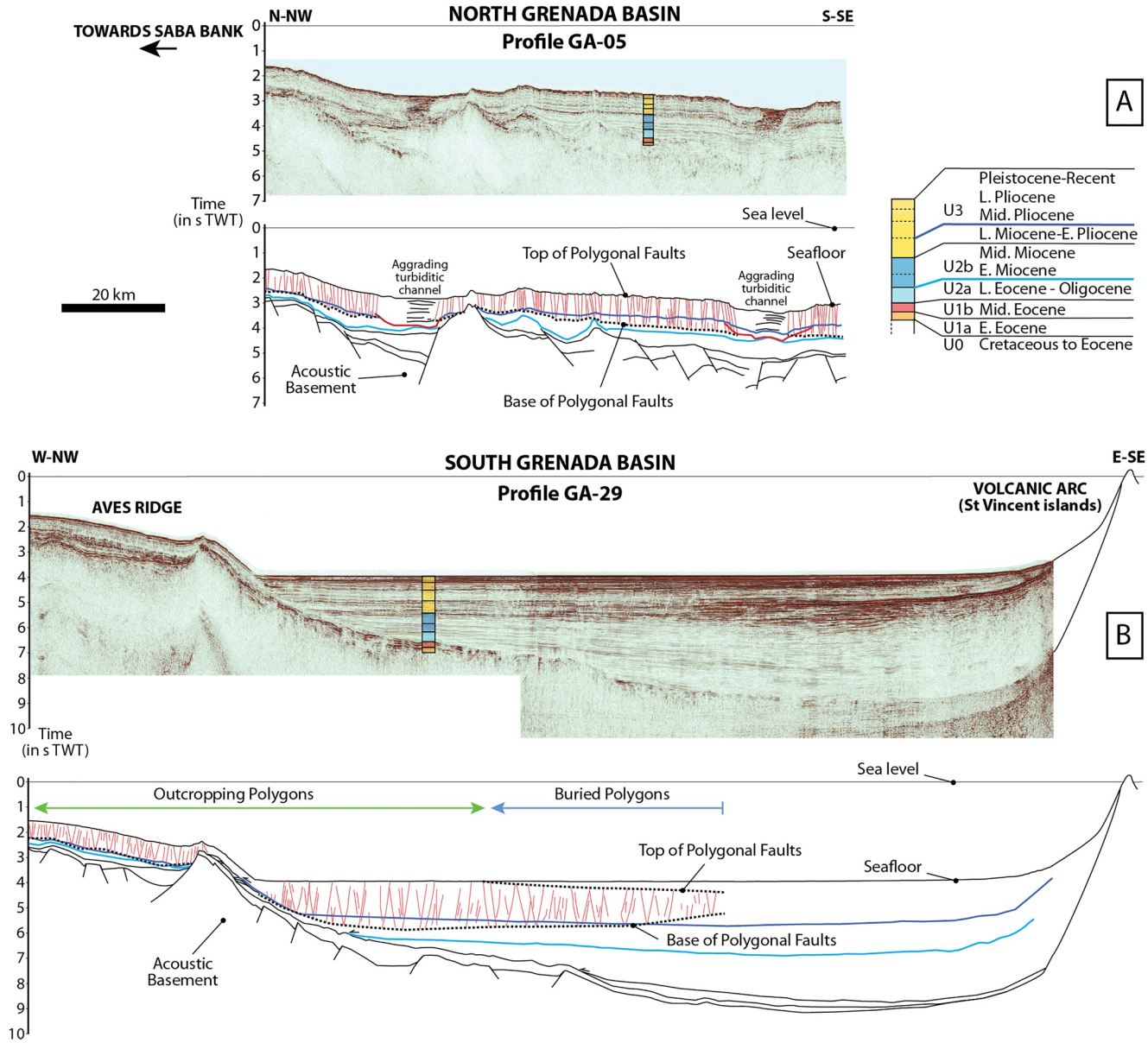

Figure 8. (a) Seismic profile GA-05 and its line-drawing displaying PFS in the NGB. The polygonal faults do not develop where deep aggrading turbiditic channels are present. PFS is getting thicker southward affecting almost all unit U2. Units U0 to U3 were correlated on GARANTI seismic data from previous studies and ODP/DSDP wells (Garrocq et al., 2021); (b) seismic profile GA-29 and its line-drawing displaying PFS in the SGB. In both the western part of the SGB and the Aves Ridge, PF are reaching the seafloor. The base of PFS varies from west to east generally affecting the top of U2. In the eastern part of the SGB PFS is thinning eastward (both the top and the base of PFS are crosscutting stratigraphic horizons) and abruptly ends 40–70 km off the volcanic arc.

However, the PFS abruptly ends at the toe of the Saba Bank (not shown in this study but visible on profile GA-15C in Cornée et al., 2021).

In the western part of the SGB, the PFS are affecting unit U3 (Figure 8b) and giant polygons are cropping out at the seabed. The base of PFS is not concordant with the base of unit U3 and it is undulating over the Grenada Basin within the top of unit U2, depending on the depth at which the faults have propagated downward. In the center of the SGB the PFS do not reach the seafloor nor unit U2 where the PFS appears buried (500 ms TWT below seafloor) and thinner (700 ms TWT) defining a lenticular shape. The PFS abruptly ends eastward at a distance of ~40–70 km from the LAA. On the Aves ridge, the PFS appears thinner by a factor of 2, which is correlated with thinner sedimentary sequences.

The total area covered by both outcropping and buried polygonal faults is about 75,000 km^2 (55,000 + 20,000 km^2 respectively), defining a crescent shape more or less concordant with the shape of the Grenada Basin (Figure 1).

3. Discussion

3.1. Polygonal Faults Orientations Versus Creep Deformation

The main hypothesis for polygonal faults formation considers an internal fluid pressure and a finite bed length extension inducing the development of conjugate subvertical fault planes with extensional offsets (i.e., apparent normal faults) due to a local bulk volume loss of pore fluids, leading to a partly compacted thinner interval (Cartwright & Lonergan, 1996; Gay et al., 2004; Shin et al., 2008). Burial and sediment loading are not common processes in normal fault formation, probably because soft sediments like clays have a specific weak rheological behavior. However, the elastic deformation of clay-rich sediments in a slope leads to the formation of discrete faults due to a creep mechanism, defined as slow gravity-driven downslope motion and deformation (Hill et al., 1982; Mulder & Cochonat, 1996; Shillington et al., 2012). Downslope motion occurs by the development of shear planes along or across stratigraphic boundaries. The dominant orientation of short axes of best-fit ellipses calculated from the center-to-center method suggests the interaction of gravity-driven shearing of the compacting interval. Internal fluid pressure and volumetric contraction of clay induce a horizontal stress tension and then could promotes radial tension reaching the extensional failure along a Griffith-type conventional envelope. However, this process assumes that (a) the faulted material has a common frictional envelope, (b) the lithostatic stress state prior to faulting due to compaction was sub-critical (i.e., close to shear failure), and/or (c) the stress tension related to the volumetric change is large enough. In such unlithified and uncompacted clay sediments, the coefficient of Earth pressure at rest (Ko) is generally large (0.45–0.8) implying little differential stress due to the vertical loading (Earl, 1997; James, 2006). This suggests that a high horizontal tension due to internal fluid pressure and contraction is needed to get the Griffith failure envelope (Cartwright & Lonergan, 1996), coupled to an external extension (Bureau et al., 2013; Laurent et al., 2012), probably due to the creep deformation of subseafloor sediments. Thus, the stress state will easily cause aligned extensional failure with minor shearing component due to the burial and increasing lithostatic pressure (Cosgrove, 1997). This model suggests that progressive sediment loading is the main driver in the initiation and propagation of subvertical polygonal faults (Gay & Berndt, 2007; Gay et al., 2004; Reiche et al., 2011). Clausen et al. (1999) have suggested that PF developed within a broadly polygonal array due to gravitational sliding influenced by far-field tectonic stresses at a regional scale. However, Wrona et al. (2017) have recently suggested that such processes played no or an imperceptible role in the growth of this specific system. Ghalayini et al. (2017) have also proposed that the distribution of PFS in the Levant Basin could be used as an indicator for delimiting clastic reservoirs, suggesting that the orientation of PF may be influenced by the regional stress field. The analysis of the orientation of the PF in the Grenada basin shows that they are more controlled by the local main slope such as in the Lower Congo Basin where the orientation of PF is controlled by the regional slope (Gay et al., 2004) or in the Angola basin where PF are perturbed by salt diapirism (Ho et al., 2018). So, the development of PFS at the seabed could thus be indicative of the present-day creep deformation of slope sediments, giving a local state of stress within the sub-seafloor (Ho et al., 2018; Jitmahantakul et al., 2020; Tuckwell et al., 2003).

In the NGB, the best-fit ellipses show a similar short axis orientation of N40°E in both areas A and B, meaning that all polygons are contracting following the same major direction. It is now commonly admitted that such direction of contraction is parallel to the minimum principal stress σ3 (Ho et al., 2018), which represent a direction of minimum extension within shallow sediments. So, we assume here that the PFS is currently in extension following one major direction of N40°E. Since Late Miocene the forearc domain has undergone a regional subsidence and a NE-SW extension evidenced in the Northern Lesser Antilles (Boucard et al., 2021) and in the intra-arc Kalinago Basin (Cornée et al., 2021). The N40°E orientation evidenced from polygon shapes thus may indicate that the PF in the upper sedimentary cover (unit U3 at least) have recorded such extension in the backarc. This is possibly explained by thermal relaxation related to the cessation of arc activity in the northeastern LAA (Jany et al., 1990; MacPhee et al., 1989; Philippon, van Hinsbergen, et al., 2020) and/or possibly by tectonics influence of subduction dynamics (Boucard et al., 2021; Philippon, van Hinsbergen, et al., 2020). However, the more recent and continuous subsidence since Late Miocene–Early Pliocene can explain shallower depths of both the present-day seafloor and the base of unit U3, with an average depth of 2 s TWT (Figure 9a), and a constant thickness of unit U3 of about 0.7–0.8 s TWT, indicating a homogeneous subsidence in the entire area with no

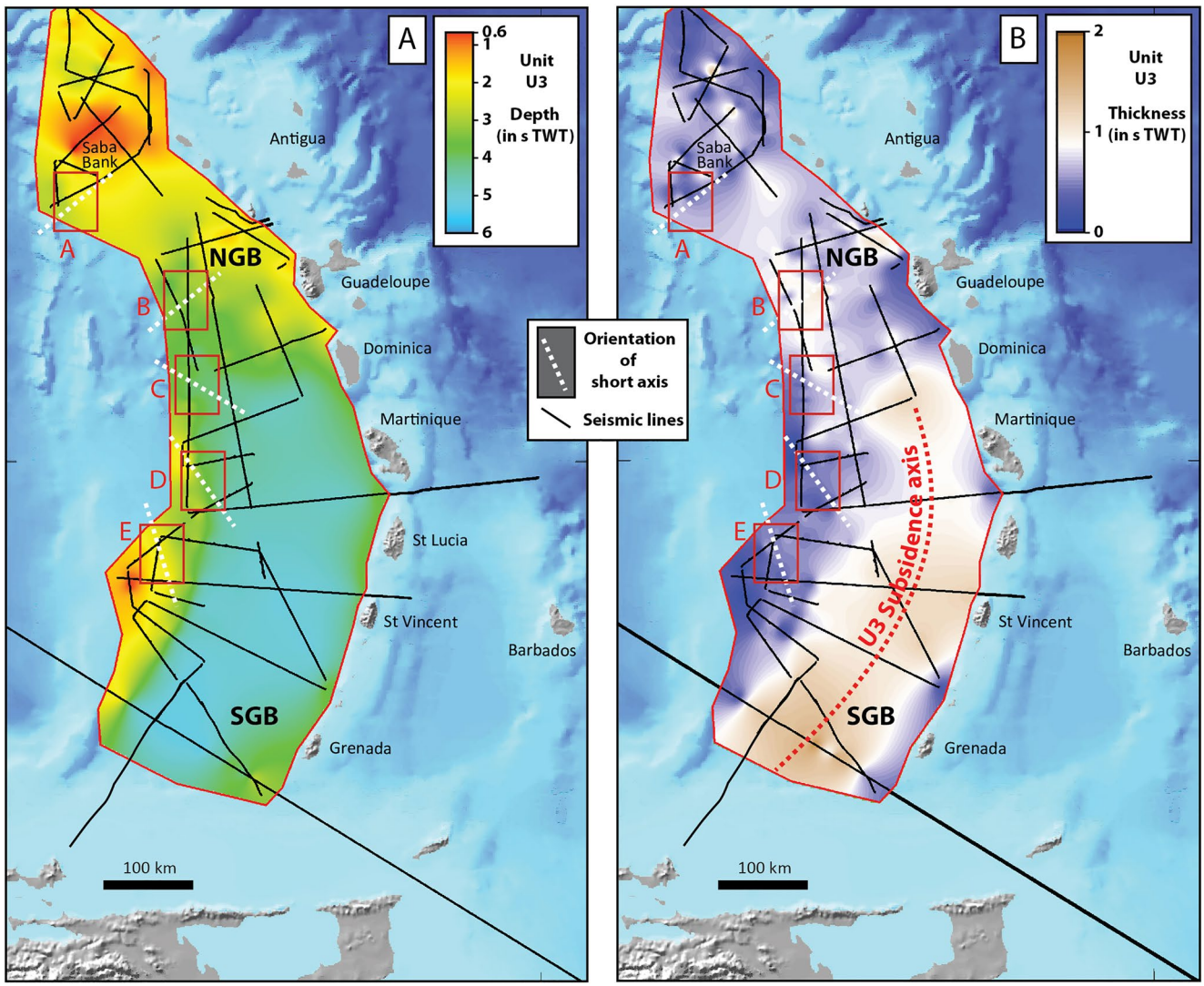

Figure 9. (a) Isochron map of the base of U3 displaying a crescent shape following the LAA. There is a sharp change west off Dominica where U3 is strongly deepening of ~3 s TWT. From Dominica to the south of Grenada Island the base of U3 is slightly deepening to reach ~5,5 s TWT. U3 is very shallow on Saba Bank and on top of the Aves Ridge. (b) Isopach map of U3 showing a homogeneous thickness in the NGB. In the SGB, U3 progressively thickens southward, indicating a differential subsidence between north and south.

major slope orientation except in the vicinity of emerged volcanic islands and around Saba Bank (Figure 9b). In the NGB, even if the best-ellipse has evidenced a short axis oriented N40°E, the polygons display a very regular shape. At this stage there is no clear evidence that the extension identified in the forearc may have propagated in the backarc, being responsible of the orientation of PF during their development. The measured seabed polygons could also be primarily related to internal isotropic contraction of the host strata due to a homogeneous burial in the area, as commonly seen in most layer-bound PFS (Wrona et al., 2017).

In the SGB, the subsidence has significantly increased from Late Miocene to present, possibly explained by a southeastward regional tilting and/or a greater sediment compaction in response to sediment loading in the basin (Garrocq et al., 2021). The base of unit U3 is characterized by a sharp change in average depth from 2 to 5 s TWT west off Dominica island and a slight deepening to the South where it reaches about 6 s TWT west off Grenada island (Figure 9a). However, the isopach map of unit U3 shows a curved NE-SW depocenter with a maximum thickness of 2,3 km in the southwest indicating a higher subsidence rate in the south. In this area the calculated best-fit ellipses from polygons show a change in direction of the short axis, indicating varying orientations of PF progressively turning toward the center of the SGB where the curved depocenter of unit U3 follows the curvature

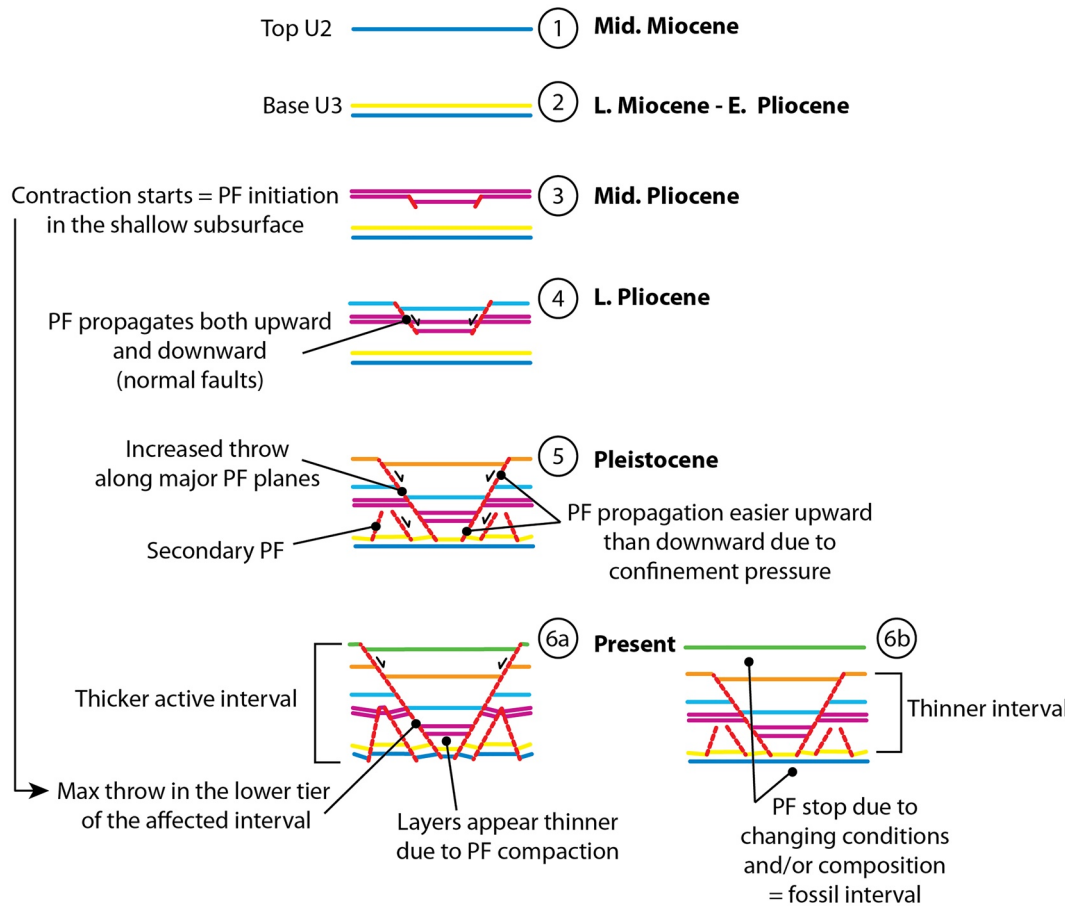

Figure 10. Schematic sketch illustrating the initiation and propagation of PF starting in the sub-seafloor in the Grenada Basin. PFS started at the transition between Early and Middle Pliocene. They are then propagating both upward and downward during sedimentation and as long as the sediment composition remains clay- and smectite-rich and the extension is large enough to allow proper contraction of sediments.

of the modern volcanic arc (Figure 9b). The major faults identified in the SGB (Aitken et al., 2011; Garrocq et al., 2021; Pindell & Barrett, 1990; Pindell & Kennan, 2009; Speed & Westbrook, 1984) do not seem to control the orientation of PF. Both the depth map and the isopach map of unit U3 indicate that the main slope oriented toward the depocenter is driving the orientation of PF. This is most probably due to the creep deformation of slope sediments toward the center of the basin.

3.2. Factors Controlling the Development of Polygonal Faults

Lithological analyses conducted on wells penetrating PFS in other basins show that the amount of shrinkage in layers appears to increase as the grain size decreases and smectite content increases (Dewhurst et al., 1999; Gay & Berndt, 2007). This composition forms a fine texture of flocculated particles, 2 μm in size, submitted to shrinkage upon drying leaving voids that are about 5 μm in width (Forsberg & Locat, 2005). This process occurs at a microscale, and could explain (a) the spontaneous contraction of mud-dominated sediments, leading to the formation of normal discrete faults at a wider scale and (b) the development of polygonal faults outcropping at the seabed, meaning that the volumetric contraction can form during early compaction, leading to a rapid bulk volume loss.

The PF initiation and propagation in the Grenada Basin can be summarized in an evolutionary model taking into account their morphology both at the seabed and on seismic profiles (Figure 10). Unit U2 was fed by clastic metamorphic material coming from the Orinoco delta while it was oriented NS, which is not compatible with spontaneous volumetric sediment contraction at seabed (stage 1). During Late Miocene the lateral shift of the

Orinoco River on the eastern flank of the LAA has limited the coarser metamorphic material input into the Grenada Basin (Diaz de Gamero, 1996; Escalona & Mann, 2011; Xie et al., 2010). The sediments at the base of unit U3 were more and more fed by smectite-rich sediments derived from the volcanic arc and/or coming from the South American continent through the CBW current (stage 2). The contraction started during the Middle Pliocene as clay-rich sediments were shallow buried (stage 3). The process of contraction has gone on as long as sediments deposited at the seabed had the composition required for PF development (Gay & Berndt, 2007; Jackson et al., 2014). Increased dewatering during burial implied more displacement along faults (Gay et al., 2004; Jitmahantakul et al., 2020), which would continue to grow as long as the dewatering cell contracted volumetrically (stage 4). The PF propagated both upward and downward although the progressive reduction in bed length through contraction was balanced by an incremental increase in the amount of displacement distributed along the faults (stage 5). Fault propagation is much easier toward the seabed than at depth due to the confinement pressure (Laurent et al., 2012), and the maximum throw along major PF planes is always found in the lower tier of the affected interval (Figure 4). At depth, secondary faults are initiated due to sediment loading in order to better drain the center of polygons (stage 5). They display lower amount of displacement than the major polygonal faults at the same stratigraphic level, confirming that the nucleation of PF occurred where/when the throw is maximum (i.e., Middle Pliocene) (stage 6a). The kinematic model of polygonal fault growth in which the propagation of faults is discontinuous during basin infilling leads to a 4D interpretation of the whole polygonal faut system. In the eastern part of the Grenada Basin, the PFS appears buried and it is thinning eastward, cross-cutting stratigraphic horizons. It can be considered as a fossil interval (stage 6b), whereas polygonal faulting remains active to the west and although the initiation point is at the same stratigraphic level both in east and west. This could reflect that the western area remains dominated by clay- and smectite-rich sedimentation, whereas the eastern area has received different lithologies. Flank collapse events have occurred all along the LAA, resulting in debris avalanches, some of them involving large volumes of material (Brunet et al., 2016; Deplus et al., 2001). A striking characteristic of the deposits in the Grenada Basin is the presence of a thick chaotic unit in seismic data, about 250 ms TWT in thickness, west off emerged islands in the deep basin. Some of the debris avalanches have evolved into debris flows and turbidity currents, feeding the eastern deep basin with coarser material (Deplus et al., 2001). At this point, the change in sediment input (and composition) seems the most probable cause for lack of PF formation in the east Grenada Basin.

3.3. Evolutionary Model of Polygonal Faults in the Grenada Basin

Major differences in depths, morphologies and PF between the NGB and the SGB are evidenced along a NS profile (GH) (Figure 11):

> The basin infilling is controlled by the available space for sedimentation. Due to repeated episodes of uplift and emersion in the north (Cornée et al., 2021; Philippon, Cornée, et al., 2020), the thickness of the sedimentary cover is relatively thin with a maximum of about 3 s TWT south of Saba Bank and west of Antigua (Figures 11a). Unit U3 appears isopachous, indicating that the present-day subsidence is homogeneous in the area. The continuous subsidence in the south since Eocene has led to a very thick sedimentary cover of about 6 s TWT between the Aves Ridge and the Grenada Island. Unit U3 is thickening southward with a relative flat seabed, indicating an actual differential subsidence which is stronger in the south (Garrocq et al., 2021) (Figures 11a).

> Classical normal faults usually propagate parallel to the principal stress σ1, while hydraulic fractures open in parallel to the intermediate horizontal stress σ2 and against the minimum principal stress σ3 (Cosgrove, 1995). However, PFS do not follow such behavior due to the anisotropy of unlithified cohesive fine-grained sediments and the anisotropic stress attributed to perturbations of the creep deformation can control the PF orientations (Carruthers et al., 2013; Ho et al., 2018). In sedimentary basins, σ1 is generally vertical and corresponds to the lithostatic vertical stress (σv) and we assume here that σ2 and σ3 are respectively perpendicular and parallel to the short axis of best fit ellipses obtained from the center-to-center method. In the north, the PFS abruptly ends at the toe of Saba Bank, a lithified reefal and red algal platform (Cornée et al., 2021) in which PF cannot develop (Figures 11b). PF are possibly controlled by a general N40°E extension of the present-day backarc basin, but they are most probably controlled by the homogeneous subsidence in the area leading to sub-isotropic PF. In the south, PF are following the deepest point of subsidence actually toward the south (Figures 11b). The active interval of

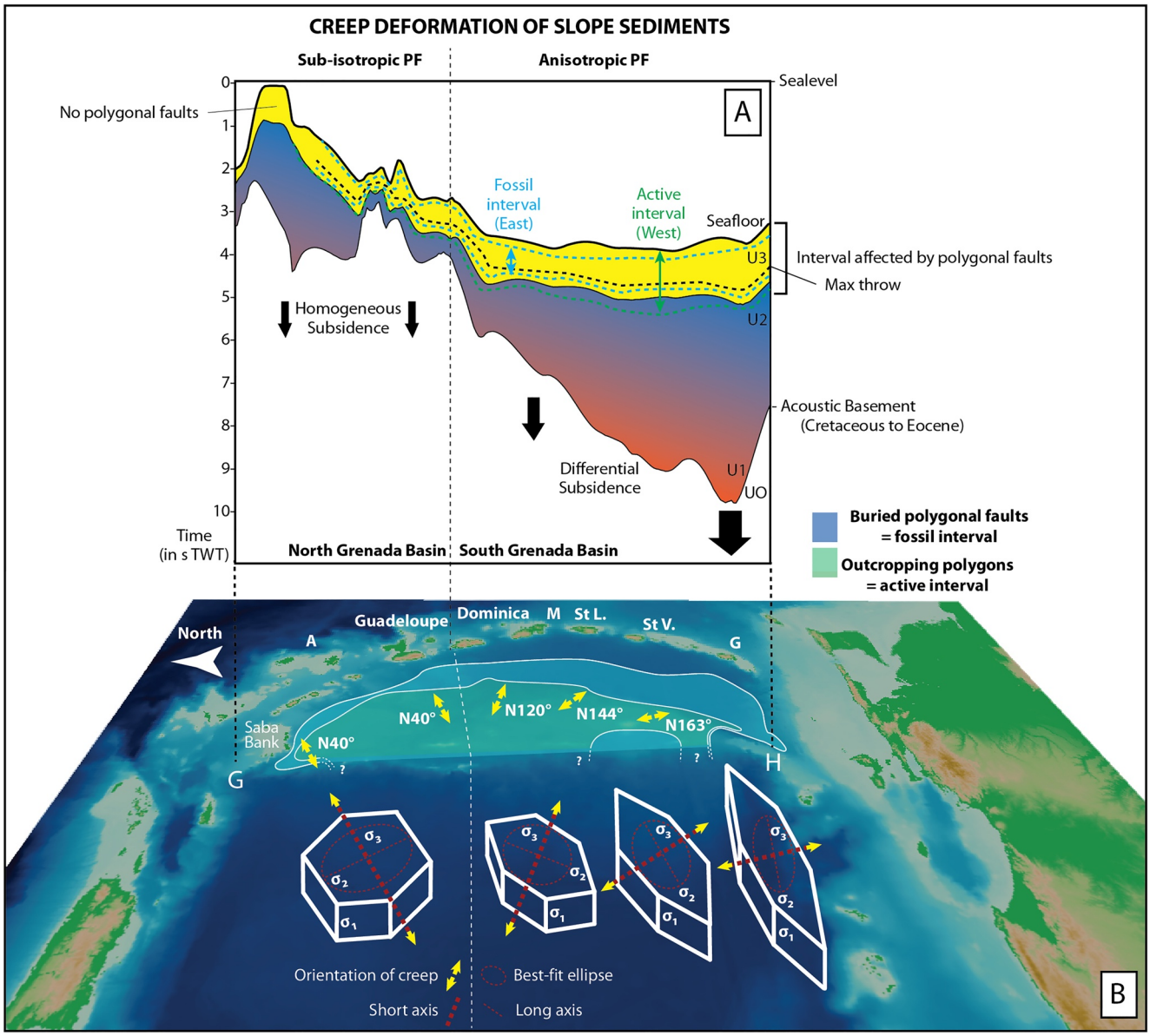

Figure 11. (a) Synthetic profile (parallel to the volcanic arc) of PF occurrence in the Grenada Basin. Between north and south the change in depths, morphologies and polygonal faults orientations is sharp, corresponding to both tectonic domains in the north Grenada Basin and the south Grenada Basin (SGB). (b) The short axes of the ellipses extracted from the center-to-center method are parallel to the orientation of extension in unit U3. It may be related to the minimum principal stress σ3, representing the main orientation of volumetric contraction of sediments. σ1 and σ2 orientations are deduced from the orientation of σ3. The orientation of σ3 is N40°E and remains constant in the NGB, whereas it is turning (N120°E to N144°E to N163°E) in the SGB, in the direction of the U3 depocenter. Giant seabed polygons in the Grenada Basin and the underlying polygonal fault system may represent markers of creep deformation of slope sediments.

PF has continued growing until the present day in the center and in the west of the Grenada Basin whereas it has stopped or never developed in the east due to coarser and/or less smectite-rich input coming from the active LAA.

>The basement remains high in the NGB, reaching a maximum of about 4 s TWT in depth, although it is strongly deepening in the SGB, reaching a maximum of 10 s TWT (Figures 11a). The different subsidence histories have strongly influenced the architecture of both basins with the SGB deepening toward a curved depocenter more or less parallel to the volcanic arc whereas the NGB remains relatively flat and high (Figures 11b). The boundary between both domains is estimated to be west off Dominica island. PFS have developed in response to burial conditions and slope processes and they actually display very different shape and organization in both domains.

4. Conclusion

A regional acquisition of seismic data, multibeam imagery at a basin scale and seabed grab cores provided new insights on the recent Grenada Basin slope processes and improved the understanding of post-depositional processes occurring in PFS. We have identified giant seabed polygons covering the largest area ever found on Earth, with a surface of ~55,000 km^2, and even up to 75,000 km^2 taking into account those which do not reach the seafloor in the center and the eastern Grenada Basin. Moreover, the western extent of the PFS area is limited by our investigation area but we suspect that most of the Aves Ridge and even its western flank is concerned.

Surprisingly, different orientations of polygons have been found in both the NGB and the SGB. The polygons are very regular in the north, whereas they are more elongated in the south. The graphical center-to-center method applied to seabed polygons provided best-fit ellipses with short axes parallel to the regional extension. In the NGB short axes of best-fit ellipses are oriented N40°E and they are parallel to a general NE-SW extension evidenced in the forearc and the Kalinago basins. However, we don't have any evidence that such extension has propagated in the backarc. Due to the regular shape of polygons, the PF have most probably formed in response to isotropic contraction of sediments during shallow burial. This is possibly due to a homogeneous subsidence in the area since middle Pliocene leading to a relatively flat and high NGB. In the SGB, short axes are progressively rotating toward the south, where units U2 and U3 are thicker and deeper, probably due to an increased subsidence from Late Miocene to present and with a higher subsidence rate in the south. PF have anisotropically developed in response to creep deformation of slope sediments sliding toward the depocenter.

In both cases, these observations show that PFS are not directly influenced by a regional state of stress due to tectonic regimes. The NGB and the SGB are the result of two different subsidence histories leading to different basin morphologies and PFS have only recorded local state of stress on different slopes, probably due to creep deformation. Further investigations, including extensive seismic acquisition and sediment sampling, must be considered in order to completely map the extent of both active and fossil/buried PFS in the entire Aves Ridge area.

Data Availability Statement

Multichannel seismic processing was performed with Geovation software of CGG and Seismic Unix. All geophysical data and GARANTI cruise data are available on demand at SISMER (www.ifremer.fr/sismer/).

Acknowledgments
This work was supported by the INSU TelluS-SYSTER grant call 2017, the GAARAnti project (ANR-17-CE31-0009), the GARANTI Cruise (2017). We are indebted to Saba Bank Resources N.V. and managing director Clark Gomes-Casseres for the provision of seismic lines of the Saba Bank. We gratefully thank the captain and crew *of R/V L'Atalante,* as well as the technical staff of Genavir for having successfully completed the acquisition of seismic data and dredge samples during the GARANTI cruise (https://doi.org/10.17600/17001200).

References

Aitken, T., Mann, P., Escalona, A., & Christeson, G. L. (2011). Evolution of the Grenada and Tobago basins and implications for arc migration. *Marine and Petroleum Geology*, *28*(1), 235–258. https://doi.org/10.1016/j.marpetgeo.2009.10.003

Allen, R. W., Collier, J. S., Stewart, A. G., Henstock, T., Goes, S., Rietbrock, A., & the VoiLA Team. (2019). The role of arc migration in the development of the Lesser Antilles: A new tectonic model for the Cenozoic evolution of the eastern Caribbean. *Geology*, *47*(9), 891–895. https://doi.org/10.1130/G46708.1

Audemard, F. A., Keith, J. H., Lorente, M. A., & Pindell, J. L. (2009). Key issues on the post-Mesozoic southern Caribbean Plate boundary. *Geological Society - Special Publications*, *328*, 569–586. https://doi.org/10.1144/SP328.23

Bader, R. G., Gerard, R. D., Benson, W. E., Bolli, H. M., Hay, W. W., Rothwell, W. T., et al. (1970). Initial reports of the deep sea drilling project, site 30. Ocean drilling program. https://doi.org/10.2973/dsdp.proc.4.1970

Beck, C., Ogawa, Y., & Dolan, J. (1990). Eocene paleogeography of the southeastern Caribbean: Relations between sedimentation on the Atlantic abyssal plain at site 672 and evolution of the South America margin. In A. Mascle, & J. C. Moore (Eds.), *Proceedings of the ocean drilling program, scientific results* (Vol. 110, pp. 7–15). https://doi.org/10.2973/odp.proc.sr.110.120.1990

Berndt, C., Jacobs, C., Evans, A., Gay, A., Elliott, G., Long, et al. (2012). Kilometre-scale polygonal seabed depressions in the Hatton Basin, NE Atlantic Ocean: Constraints on the origin of polygonal faulting. *Marine Geology*, *332*(334), 126–133. https://doi.org/10.1016/j.margeo.2012.09.013

Boschman, L. M., van Hinsbergen, D. J., Torsvik, T. H., Spakman, W., & Pindell, J. L. (2014). Kinematic reconstruction of the Caribbean region since the Early Jurassic. *Earth-Science Reviews*, *138*, 102–136. https://doi.org/10.1016/j.earscirev.2014.08.007

Boucard, M., Marcaillou, B., Lebrun, J.-F., Laurencin, M., Klingelhoefer, F., Laigle, M., et al. (2021). Paleogene V-shaped basins and Neogene subsidence of the Northern Lesser Antilles Forearc. *Tectonics*, *40*, e2020TC006524. https://doi.org/10.1029/2020TC006524

Bouysse, P., Andreieff, P., Richard, M., Baudron, J., Mascle, A., Maury, R., et al. (1985). Aves swell and northern Lesser Antilles Ridge: Rock-dredging results from ARCANTE 3 cruise. In A. Mascle (Ed.), *Caribbean geodynamics* (pp. 65–76). Editions Technip.

Bouysse, P., & Westercamp, D. (1990). Subduction of Atlantic aseismic ridges and Late Cenozoic evolution of the Lesser Antilles island arc. *Tectonophysics*, *175*, 349–380. https://doi.org/10.1016/0040-1951(90)90180-g

Bowles, F. A., & Fleischer, P. (1985). Orinoco and Amazon River sediment input to the eastern Caribbean Sea. *Marine Geology*, *68*, 53–72. https://doi.org/10.1016/0025-3227(85)90005-2

Brunet, M., Le Friant, A., Boudon, G., Lafuerza, S., Talling, P., Hornbach, M., and the IODP Expedition 340 Science Party. (2016). Composition, geometry, and emplacement dynamics of a large volcanic island landslide offshore Martinique: From volcano flank-collapse to seafloor sediment failure? *Geochemistry, Geophysics, Geosystems*, *17*(3), 699–724. https://doi.org/10.1002/2015GC006034

Bureau, D., Mourgues, R., Cartwright, J., Foschi, M., & Abdelmalak, M. M. (2013). Characterization of interactions between a pre-existing polygonal fault system and sandstone intrusions and the determination of paleo-stresses in the Faroe-Shetland basin. *Journal of Structural Geology*, *46*, 186–199. https://doi.org/10.1016/j.jsg.2012.09.003

Carey, S., & Sigurdsson, H. (1978). Deep-sea evidence for distribution of tephra from the mixed magma eruption of the Soufriere of St. Vincent, 1902: Ash turbidites and air fall. *Geology*, *6*, 271–274. https://doi.org/10.1130/0091-7613(1978)6<271:defdot>2.0.co;2

Carey, S., & Sigurdsson, H. (1984). A model of volcanogenic sedimentation in marginal basins. *Geological Society Special Publication*, *16*, 37–58. https://doi.org/10.1144/gsl.sp.1984.016.01.04

Carruthers, D., Cartwright, J., Jackson, M. P., & Schutjens, P. (2013). Origin and timing of layer-bound radial faulting around North Sea salt stocks: New insights into the evolving stress state around rising diapirs. *Marine and Petroleum Geology*, *48*, 130–148. https://doi.org/10.1016/j.marpetgeo.2013.08.001

Cartwright, J. (2011). Diagenetically induced shear failure of fine-grained sediments and the development of polygonal fault systems. *Marine and Petroleum Geology*, *28*(9), 1593–1610. https://doi.org/10.1016/j.marpetgeo.2011.06.004

Cartwright, J., & Dewhurst, D. (1998). Layer-bound compaction faults in finegrained sediments. *Geological Society of America Bulletin*, *10*(10), 1242–1257. https://doi.org/10.1130/0016-7606(1998)110<1242:LBCFIF>;2.2.3.CO

Cartwright, J., & Lonergan, L. (1996). Volumetric contraction during the compaction of mudrocks: A mechanism for the development of regional-scale polygonal fault systems. *Basin Research*, *8*, 183–193. https://doi.org/10.1046/j.1365-2117.1996.01536.x

Cartwright, J. A. (1994). Episodic basin-wide hydrofracturing of overpressured Early Cenozoic mudrock sequences in the North Sea Basin. *Marine and Petroleum Geology*, *11*(5), 587–607. https://doi.org/10.1016/0264-8172(94)90070-1

Cattaneo, A., Correggiari, A., Marsset, T., Thomas, Y., Marsset, B., & Trincardi, F. (2004). Seafloor undulation pattern on the Adriatic shelf and comparison to deep-water sediment waves. *Marine Geology*, *213*, 121–148. https://doi.org/10.1016/j.margeo.2004.10.004

Christeson, G. L., Mann, P., Escalona, A., & Aitken, T. J. (2008). Crustal structure of the Caribbean–northeastern South America arc-continent collision zone. *Journal of Geophysical Research*, *113*, B08104. https://doi.org/10.1029/2007JB005373

Clausen, J. A., Gabrielsen, R. H., Reksnes, P. A., & Nysaether, E. (1999). Development of intraformational (Oligocene–Miocene) faults in the northern North Sea: Influence of remote stresses and doming of Fennoscandia. *Journal of Structural Geology*, *21*(10), 1457–1475. https://doi.org/10.1016/S0191-8141(99)00083-8

Clausen, J. A., & Korstgård, J. A. (1993). Small scale faulting as an indicator of deformation mechanism in the Tertiary sediments of the northern Danish Central Trough. *Journal of Structural Geology*, *15*, 1343–1358. https://doi.org/10.1016/0191-8141(93)90107-l

Cornée, J-J., Münch, P., Philippon, M., BouDagher-Fadel, M., Quillévéré, F., Melinte-Dobrinescu, M., & the GARANTI and ANTITHESIS Scientific Parties. (2021). Lost islands in the northern Lesser Antilles: A possible milestone in the Cenozoic dispersal of terrestrial organisms between South-America and the Greater Antilles. *Earth Sciences Reviews*, *217*, 103617. https://doi.org/10.1016/j.earscirev.2021.103617

Corredor, J., Moreli, J., Lopez, J., Capella, J., & Armstrong, R. (2004). Cyclonic eddy entrains Orinoco river plume in Eastern Caribbean. *EOS Transactions – American Geophysical Union*, *85*(20), 197–201. https://doi.org/10.1029/2004eo200001

Cosgrove, J. (1995). The expression of hydraulic fracturing in rocks and sediments. *Geological Society Special Publication*, *92*, 187–196. https://doi.org/10.1144/gsl.sp.1995.092.01.10

Cosgrove, J. W. (1997). Hydraulic fractures and their implications regarding the state of stress in a sedimentary sequence during burial. In S. Sengupta (Ed.), *Evolution of geological Structures in micro- to macro-scales*. Springer. https://doi.org/10.1007/978-94-011-5870-1_2

Davies, R. J., Ireland, M. T., & Cartwright, J. (2009). Differential compaction due to irregular topology of a diagenetic reaction boundary: A new mechanism for the formation of polygonal faults. *Basin Research*, *21*, 354–359. https://doi.org/10.1111/j.1365-2117.2008.00389.x

DeMets, C., Jansma, P. E., Mattioli, G. S., Dixon, T. H., Farina, F., Bilham, R., et al. (2000). GPS geodetic constraints on Caribbean-North America plate motion. *Geophysical Research Letters*, *27*(3), 437–440. https://doi.org/10.1029/1999GL005436

Deplus, C., Le Friant, A., Boudon, G., Komorowski, J-C., Villemant, B., Harford, C., et al. (2001). Submarine evidence for large-scale debris avalanches in the Lesser Antilles Arc. *Earth and Planetary Science Letters*, *192*(2), 145–157. https://doi.org/10.1016/S0012-821X(01)00444-7

Desprairies, A., & Bonnot-Courtois, C. (1980). Relation entre la composition des smectites d'altération sous-marine et leurs cortèges de terres rares. *Earth and Planetary Science Letters*, *48*(1), 124–130. https://doi.org/10.1016/0012-821x(80)90175-2

Deville, E., Mascle, A., Callec, Y., Huyghe, P., & Lallemant, S. (2015). Tectonics and sedimentation interactions in the east Caribbean subduction zone; an overview from the Orinoco Delta and the Barbados accretionary prism. *Marine and Petroleum Geology*, *64*, 76–103. https://doi.org/10.1016/j.marpetgeo.2014.12.015

Dewhurst, D. N., Cartwright, J., & Lonergan, L. (1999). The development of polygonal fault systems by syneresis of colloidal sediments. *Marine and Petroleum Geology*, *16*, 793–810. https://doi.org/10.1016/s0264-8172(99)00035-5

Diaz de Gamero, M. L. (1996). The changing course of the Orinoco River during the Neogene: A review. *Palaeogeography, Palaeoclimatology, Palaeoecology*, *123*, 385–402. https://doi.org/10.1016/0031-0182(96)00115-0

Earl, E. (1997). Assessment of the behaviour of field soils during compression. *Journal of Agricultural Engineering Research*, *68*, 147–157. https://doi.org/10.1006/jaer.1997.0192

Escalona, A., & Mann, P. (2011). Tectonics, basin subsidence mechanisms, and paleogeography of the Caribbean-South American plate boundary zone. *Marine and Petroleum Geology*, *28*, 8–39. https://doi.org/10.1016/j.marpetgeo.2010.01.016

Forsberg, C. F., & Locat, J. (2005). Mineralogical and microstructural development of the sediments on the Mid-Norwegian margin. *Marine and Petroleum Geology*, *22*(1–2), 109–122. https://doi.org/10.1016/b978-0-08-044694-3.50013-5

Fox, P. J., Schreiber, E., & Heezen, B. C. (1971). The geology of the Caribbean crust: Tertiary sediments, granitic and basic rocks from the Aves Ridge. *Tectonophysics*, *12*(2), 89–109. https://doi.org/10.1016/0040-1951(71)90011-4

Fry, N. (1979). Random point distributions and strain measurement in rocks. *Tectonophysics*, *60*, 89–105. https://doi.org/10.1016/0040-1951(79)90135-5

Garrocq, C., Lallemand, S., Marcaillou, B., Lebrun, J-F., Padron, C., Klingelhoefer, F., & the GARANTI cruise team. (2021). Genetic relations between the Aves Ridge and the Grenada back-arc basin, East Caribbean Sea. *Journal of Geophysical Research: Solid Earth*, *126*, e2020JB020466. https://doi.org/10.1029/2020JB020466

Gay, A., & Berndt, C. (2007). Cessation/reactivation of polygonal faulting and effects on fluid flow in the Vøring Basin, Norwegian Margin. *Journal of the Geological Society of London*, *164*, 129–141. https://doi.org/10.1144/0016-76492005-178

Gay, A., Lopez, M., Berndt, C., & Séranne, M. (2007). Geological controls on focused fluid flow associated with seafloor seeps in the Lower Congo Basin. *Marine Geology*, *244*, 68–92. https://doi.org/10.1016/j.margeo.2007.06.003

Gay, A., Lopez, M., Cochonat, P., & Sermondadaz, G. (2004). Polygonal faults–furrows system related to early stages of compaction—Upper Miocene to present sediments of the Lower Congo Basin. *Basin Research*, *16*, 101–116. https://doi.org/10.1111/j.1365-2117.2003.00224.x

Ghalayini, R., & Eid, C. (2020). Using polygonal layer-bound faults as tools to delimit clastic reservoirs in the Levant Basin offshore Lebanon. *AAPG Bulletin*, *104*(3), 629–656. https://doi.org/10.1306/07151918155

Ghalayini, R., Homberg, C., Daniel, J-M., & Nader, F. H. (2017). Growth of layer-bound normal faults under a regional anisotropic stress field. *Geological Society, London, Special Publications*, *439*, 57–78. https://doi.org/10.1144/SP439.13

Gómez-García, Á. M., Meeßen, C., Scheck-Wenderoth, M., Monsalve, G., Bott, J., Bernhardt, A., et al. (2019). 3D modeling of vertical gravity gradients and the delimitation of tectonic boundaries: The Caribbean oceanic domain as a case study. *Geochemistry, Geophysics, Geosystems*, *20*(11), 5371–5393.

Goulty, N. R. (2002). Mechanics of layer-bound polygonal faulting in fine-grained sediments. *Journal of the Geological Society of London*, *159*, 239–246. https://doi.org/10.1144/0016-764901-111

Goulty, N. R. (2008). Geomechanics of polygonal fault systems: A review. *Petroleum Geoscience*, *14*, 389–397. https://doi.org/10.1144/1354-079308-781

Hansen, D. M., Shimeld, J. W., Williamson, M. A., & Lykke-Andersen, H. (2004). Development of a major polygonal fault system in Upper Cretaceous chalk and Cenozoic mudrocks of the Sable Subbasin, Canadian Atlantic margin. *Marine and Petroleum Geology*, *21*, 1205–1219. https://doi.org/10.1016/j.marpetgeo.2004.07.004

Hansen, J. P. V., Cartwright, J. A., Huuse, M., & Clausen, O. R. (2005). 3D seismic expression of fluid migration and mud remobilization on the Gjallar Ridge, offshore mid-Norway. *Basin Research*, *17*, 123–139. https://doi.org/10.1111/j.1365-2117.2005.00257.x

He, C., Tang, C., Huang, D., & Shi, S. (2010). Polygonal faults in the Sanzhao sag of the Songliao basin: Their significance in hydrocarbon accumulation. *Mining Science and Technology*, *20*, 300–305. https://doi.org/10.1016/s1674-5264(09)60202-7

Hill, P. R., Moran, K. M., & Blasco, S. M. (1982). Creep deformation of slope sediments in the Canadian Beaufort Sea. *Geo-Marine Letters*, *2*, 163–170. https://doi.org/10.1007/BF02462758

Ho, S., Hovland, M., Blouet, J-P., Wetzel, A., Imbert, P., & Carruthers, D. (2018). Formation of linear planform chimneys controlled by preferential hydrocarbon leakage and anisotropic stresses in faulted fine-grained sediments, offshore Angola. *Solid Earth*, *9*, 1437–1468. https://doi.org/10.5194/se-9-1437-2018

Holcombe, T. L., Ladd, J. W., Westbrook, G., Edgar, N. T., & Bowland, C. L. (1990). Caribbean marine geology; ridges and basin of the plate interior. In G. Dengo, & J. E. Case (Eds.), *The Caribbean region, the geology of north America* (pp. 231–260). Geological Society of America.

Ireland, M. T., Davies, R. J., Goulty, N. R., & Carruthers, D. (2011). Structure of a silica diagenetic transformation zone: The Gjallar Ridge, offshore Norway. *Sedimentology*, *58*, 424–441. https://doi.org/10.1111/j.1365-3091.2010.01170.x

Iturralde-Vinent, M. A., & MacPhee, R. D. E. (1999). Paleogeography of the Caribbean region: Implications for Cenozoic biogeography. *Bulletin of the American Museum of Natural History*. *95*.

Jackson, C., Carruthers, D., Mahlo, S., & Briggs, O. (2014). Can polygonal faults help locate deep-water reservoirs? *AAPG Bulletin*, *98*(9), 1717–1738. https://doi.org/10.1306/03131413104

James, D. M. D. (2006). Discussion on development of polygonal fault systems: A test of hypotheses. *Journal of the Geological Society of London*, *162*, 587–590. https://doi.org/10.1144/0016-764905-111

Jany, I., Scanlon, K. M., & Mauffret, A. (1990). Geological interpretation of combined seabeam, Gloria and seismic data from Anegada passage (Virgin Islands, north Caribbean). *Marine Geophysical Researches*, *12*, 173–196. https://doi.org/10.1007/bf02266712

Jitmahantakul, S., Chenrai, P., Kanjanapayont, P., & Kanitpanyacharoen, W. (2020). Seismic characteristics of polygonal faults systems in the Great South Nasin, New Zealand. *Open Geosciences*, *12*, 851–865. https://doi.org/10.1515/geo-2020-0177

Kinder, T. H., Heburn, G. W., & Green, A. W. (1985). Some aspects of the Caribbean circulation. *Marine Geology*, *68*, 25–52. https://doi.org/10.1016/0025-3227(85)90004-0

King, J. J., & Cartwright, J. A. (2020). Ultra-slow rates of polygonal fault systems. *Geology*, *48*(5), 473–477. https://doi.org/10.1130/G47221.1

Klitgord, K. D., & Grow, J. A. (1980). Jurassic seismic stratigraphy and basement structure of the western Atlantic magnetic quiet zone. *AAPG Bulletin*, *64*, 1658–1680. https://doi.org/10.1306/2f9196e3-16ce-11d7-8645000102c1865d

Ladd, J. W., & Sheridan, R. E. (1987). Seismic stratigraphy of the Bahamas. *AAPG Bulletin*, *71*(6), 719–736. https://doi.org/10.1306/94887898-1704-11d7-8645000102c1865d

Laurent, D., Gay, A., Baudon, C., Berndt, C., Soliva, R., Planke, S., et al. (2012). High-resolution architecture of a polygonal fault interval inferred from geomodel applied to 3D seismic data from the Gjallar Ridge, Vøring Basin, offshore Norway. *Marine Geology*, *332*, 134–151. https://doi.org/10.1016/j.margeo.2012.07.016

Lebrun, J-F., & Lallemand, S. (2017). GARANTI cruise, L'Atalante R/V. https://doi.org/10.17600/17001200

Le Friant, A., Lebas, E., Brunet, M., Lafuerza, S., Hornbach, M., Coussens, & the IODP 340 Expedition Science Party. (2020). Submarine landslides around volcanic islands: A review of what can be learned from the Lesser Antilles Arc. In K. Ogata, A. Festa, & G. A. Pini (Eds.), *Submarine landslides: Subaqueous mass transport deposits from outcrops to seismic profiles* (Vol. 246, pp. 277–297). Geophysical Monograph. https://doi.org/10.1002/9781119500513.ch17

Legendre, L., Philippon, M., Münch, P., Leticee, J-L., Noury, M., Maincent, G., et al. (2018). Trench bending initiation: Upper plate strain pattern and volcanism. Insights from the Lesser Antilles arc, St. Barthelemy Island, French West Indies. *Tectonics*, *37*(9), 2777–2797. https://doi.org/10.1029/2017tc004921

Li, J., Mitra, S., & Qi, J. (2020). Seismic analysis of polygonal fault systems in the Great South Basin, New Zealand. *Marine and Petroleum Geology*, *111*, 638–649. https://doi.org/10.1016/j.marpetgeo.2019.08.052

Lonergan, L., Cartwright, J., & Jolly, R. (1998). The geometry of polygonal fault in Tertiary mudrocks of the North Sea. *Journal of Structural Geology*, *20*, 529–548. https://doi.org/10.1016/s0191-8141(97)00113-2

MacDdonald, R., Hawkesworth, C. J., & Heath, E. (2000). The lesser Antilles chain: A study in arc magmatism. *Earth-Science Reviews*, *49*(1), 1–76.

MacPhee, R. D. E., Ford, D. C., & McFarlane, D. A. (1989). Pre-Wisconsinan mammals from Jamaica and models of late Quaternary extinction in the Greater Antilles. *Quaternary Research*, *31*(1), 94–106. https://doi.org/10.1016/0033-5894(89)90088-4

Mann, P. (1999). Caribbean sedimentary basins: Classification and tectonic setting from Jurassic to present. In P. Mann (Ed.), *Caribbean basins: Sedimentary basins of the world* (Vol. 4). Elsevier Science, B.V. https://doi.org/10.1016/S1874-5997(99)80035-5

Mas, A., Guisseau, D., Patrier, P., Beaufort, D., Genter, A., Sanjuan, B., et al. (2006). Clay minerals related to the hydrothermal activity of the Bouillante geothermal field (Guadeloupe). *Journal of Volcanology and Geothermal Research*, *158*, 380–400. https://doi.org/10.1016/j.jvolgeores.2006.07.010

Mas, A., Patrier, P., Beaufort, D., & Genter, A. (2003). Clay-mineral signatures of fossil and active hydrothermal circulations in the geothermal system of the Lamentin Plain, Martinique. *Journal of Volcanology and Geothermal Research*, *124*, 195–218. https://doi.org/10.1016/s0377-0273(03)00044-1

Morley, C. K., & Binazirnejad, H. (2020). Investigating polygonal fault topological variability: Structural causes vs image resolution. *Journal of Structural Geology*, *130*, 103930. https://doi.org/10.1016/j.jsg.2019.103930

Mulder, T., & Cochonat, P. (1996). Classification of offshore mass movements. *Journal of Sedimentary Research*, *66*, 43–57. https://doi.org/10.1306/d42682ac-2b26-11d7-8648000102c1865d

Münch, P., Cornee, J-J., Lebrun, J-F., Quillevere, F., Verati, C., Melinte-Dobrinescu, M., et al. (2014). Pliocene to Pleistocene vertical movements in the forearc of the Lesser Antilles subduction: Insights from chronostratigraphy of shallow-water carbonate platforms (Guadeloupe archipelago). *Journal of the Geological Society*, *171*(3), 329–341. https://doi.org/10.1144/jgs2013-005

Murray, N. A., McManus, J., Palmer, M. R., Haley, B., & Manners, H. (2018). Diagenesis in tephra-rich sediments from the Lesser Antilles Volcanic Arc: Pore fluid constraints. *Geochimica et Cosmochimica Acta*, *228*, 119–135. https://doi.org/10.1016/j.gca.2018.02.039

Neagu, R. C., Cartwright, J., & Davies, R. J. (2010). Measurement of diagenetic compaction strain quantitative analysis of fault plane dip. *Journal of Structural Geology*, *32*, 641–655. https://doi.org/10.1016/j.jsg.2010.03.010

Neill, I., Kerr, A. C., Hastie, A. R., Stanek, K. P., & Millar, I. L. (2011). Origin of the Aves Ridge and Dutch–Venezuelan Antilles: Interaction of the Cretaceous 'Great Arc' and Caribbean–Colombian Oceanic Plateau? *Journal of the Geological Society*, *168*(2), 333–348. https://doi.org/10.1144/0016-76492010-067

Oldham, A. C., & Gibbins, N. M. (1995). Lake Hope 3D: A case study. *Exploration Geophysics*, *26*, 383–394. https://doi.org/10.1071/eg995383

Packwood, R. H., & Brown, J. D. (1981). A Gaussian expression to describe ϕ(ρz) curves for quantitative electron probe microanalysis. *X-Ray Spectrometry*, *10*(3), 138–146. https://doi.org/10.1002/xrs.1300100311

Padron, C., Klingelhoefer, F., Marcaillou, B., Lebrun, J.-F., Lallemand, S., Garrocq, C., et al. (2021). Deep structure of the Grenada Basin from wide-angle seismic, bathymetric and gravity data. *Journal of Geophysical Research: Solid Earth*, *126*, e2020JB020472. https://doi.org/10.1029/2020JB020472

Parra, M., Delmont, P., Ferragne, A., Latouche, C., Pons, J. C., & Puechmaille, C. (1985). Origin and evolution of smectites in recent marine sediments of the NE Atlantique. *Clay Minerals*, *20*, 335–346. https://doi.org/10.1180/claymin.1985.020.3.06

Parra, M., Pons, J. C., & Ferragne, A. (1986). Two potential sources for Holocene clay sedimentation in the Caribbean Basin: The Lesser Antilles Arc and the South American continent. *Marine Geology*, *72*(287), 3–14. https://doi.org/10.1016/0025-3227(86)90124-6

Pautrizel, F., & Pons, J.-C. (1981). Modalités de la sédimentation au Quaternaire récent dans la Mer des Petites Antilles (Fosse de Grenade--Ride des Oiseaux--Bassin du Venezuela). *Bulletin lnstitut Géologie Bassin Aquitaine*, *30*, 239–262.

Philippon, M., Cornée, J-J., Münch, P., van Hinsbergen, D. J. J., BouDagher-Fadel, M., Gailler, L., et al. (2020). Eocene intra-plate shortening responsible for the rise of a faunal pathway in the northeastern Caribbean realm. *PLoS One*, *15*(10), e0241000. https://doi.org/10.1371/journal.pone.0241000

Philippon, M., van Hinsbergen, D., Boschman, L. M., Gossink, L., Cornée, J-J., BouDagher-Fadel, M., et al. (2020). Caribbean intra-plate deformation: Paleomagnetic evidence from St. Barthelemy Island for Post-Oligocene rotation in the Lesser Antilles forearc. *Tectonophysics*, *777*, 228323. https://doi.org/10.1016/j.tecto.2020.228323

Picard, M., Schneider, J-L., Boudon, G., & Mulder, T. (2006). Contrasting sedimentary processes along a convergent margin; the Lesser Antilles arc system. *Geo-Marine Letters*, *26*(6), 397–410. https://doi.org/10.1007/s00367-006-0046-y

Pindell, J., Kennan, L., Stanek, K. P., Maresch, W. V., & Draper, G. (2006). Foundations of Gulf of Mexico and Caribbean evolution: Eight controversies resolved. *Geológica Acta*, *4*(1–2), 303–341.

Pindell, J., Maresch, W. V., Martens, U., & Stanek, K. (2012). The Greater Antillean Arc: Early Cretaceous origin and proposed relationship to Central American subduction mélanges: Implications for models of Caribbean evolution. *International Geology Review*, *54*(2), 131–143. https://doi.org/10.1080/00206814.2010.510008

Pindell, J. L., & Barrett, S. F. (1990). Geological evolution of the Caribbean region: A plate tectonic perspective. In G. Dengo, & J. E. Case (Eds.), *The Caribbean region, the geology of north America* (pp. 405–432). Geological Society of America.

Pindell, J. L., & Kennan, L. (2009). Tectonic evolution of the Gulf of Mexico, Caribbean and northern South America in the mantle reference frame: An update. *Origin and Evolution of the Caribbean Plate*, *328*(1), 1–55. https://doi.org/10.1144/sp328.1

Reiche, S., Hjelstuen, B. O., & Haflidason, H. (2011). High-resolution seismic stratigraphy, sedimentary processes and the origin of seabed cracks and pockmarks at Nyegga, mid-Norwegian margin. *Marine Geology*, *284*(1), 28–39. https://doi.org/10.1016/j.margeo.2011.03.006

Seibert, C., Feuillet, N., Ratzov, G., Beck, C., & Cattaneo, A. (2020). Seafloor morphology and sediment transfer in the mixed carbonate siliciclastic environment of the Lesser Antilles forearc along Barbuda to St. Lucia. *Marine Geology*, *428*, 106242. https://doi.org/10.1016/j.margeo.2020.106242

Sen Gupta, B. K., Temples, T. J., & Dallmeyer, M. D. G. (1982). Diagenesis in tephra-rich sediments from the Lesser Antilles volcanic arc; pore fluid constraints. *Marine Micropaleontology*, *7*(4), 297–309. https://doi.org/10.1016/0377-8398(82)90007-x

Shillington, D., Seeber, L., Sorlien, C., Steckler, M., Kurt, H., Dondurur, D., et al. (2012). Evidence for widespread creep on the flanks of the Sea of Marmara transform basin from marine geophysical data. *Geology*, *40*, 439–442. https://doi.org/10.1130/G32652.1

Shin, H., Santamarina, J. C., & Cartwright, J. A. (2008). Contraction-driven shear failure in compacting uncemented sediments. *Geology*, *36*(12), 931–934. https://doi.org/10.1130/g24951a.1

Shin, H., Santamarina, J. C., & Cartwright, J. A. (2010). Displacement field in contraction driven faults. *Journal of Geophysical Research*, *115*(B7), 13. https://doi.org/10.1029/2009JB006572

Sigurdsson, H., Sparks, R. S. J., Carey, S. T., & Huang, T. C. (1980). Volcanogenic sedimentation in the Lesser Antilles arc. *Journal of Geology*, *88*, 523–540. https://doi.org/10.1086/628542

Speed, R. C., & Westbrook, G. K. (1984). Lesser Antilles arc and adjacent terranes. In *Atlas 10, ocean margin drilling program (marine science international)*. Woods Hole.

Sun, Q., Wu, S., Lü, F., & Yuan, S. (2010). Polygonal faults and their implications for hydrocarbon reservoirs in the southern Qiongdongnan Basin, South China Sea. *Journal of Asian Earth Sciences*, *39*, 470–479. https://doi.org/10.1016/j.jseaes.2010.04.002

Tuckwell, G. W., Lonergan, L., & Jolly, R. (2003). The control of stress history and flaw distribution on the evolution of polygonal fracture networks. *Journal of Structural Geology*, *25*, 1241–1250. https://doi.org/10.1016/s0191-8141(02)00165-7

Watterson, J., Walsh, J., Nicol, A., Neil, P. A. R., & Bretan, P. G. (2000). Geometry and origin of a polygonal fault system. *Journal of the Geological Society of London*, *157*, 151–162. https://doi.org/10.1144/jgs.157.1.151

Wrona, T., Magee, C., Jackson, C., Huuse, M., & Taylor, K. (2017). Kinematics of polygonal fault systems: Observations from the Northern North Sea. *Frontiers in Earth Sciences*, *5*, 101. https://doi.org/10.3389/feart.2017.00101

Xie, X., Mann, P., & Escalona, A. (2010). Regional provenance study of Eocene clastic sedimentary rocks within the South America-Caribbean plate boundary zone using detrital zircon geochronology. *Earth and Planetary Science Letters*, *291*(1–4), 159–171. https://doi.org/10.1016/j.epsl.2010.01.009

Ysaccis, R. (1997). Tertiary evolution of the northeastern Venezuela offshore (Thesis). Rice University. Retrieved from https://scholarship.rice.edu/handle/1911/19330